

Review

# Abatement of Greenhouse Gas Emissions from Ventilation Air Methane (VAM) Using Ionic Liquids: A Review of Experimental Methods and Modelling Approaches

Hamid Reza Rahimpour, Jafar Zanganeh \*  and Behdad Moghtaderi

Priority Research Centre for Frontier Energy Technology & Utilisation, The University of Newcastle, Callaghan, NSW 2308, Australia; hamidreza.rahimpour@newcastle.edu.au (H.R.R.); behdad.moghtaderi@newcastle.edu.au (B.M.)

\* Correspondence: jafar.zanganeh@newcastle.edu.au; Tel.: +61-2-40339335

**Abstract:** Ventilation Air Methane (VAM) refers to the release of fugitive methane ( $\text{CH}_4$ ) emissions into the atmosphere during underground coal mining operations. Growing concerns regarding the greenhouse effects of  $\text{CH}_4$  have led to a worldwide effort in developing efficient and cost-effective methods of capturing  $\text{CH}_4$ . Among these, absorption-based processes, particularly those using Ionic Liquids (ILs) are appealing due to their advantages over conventional methods. In this study, the solubility of  $\text{CH}_4$  in various ILs, expressed by Henry's law constant, is first reviewed by examining a wide range of experimental techniques. This is followed by a review of thermodynamic modelling tools such as the extended Henry's law model, extended Pitzer's model, Peng–Robinson (PR) equation of state, and Krichevsky–Kasarnovsky (KK) equation of state as well as computational (Artificial Neural Network) modelling approaches. The comprehensive analysis presented in this paper aims to provide a deeper understanding of the factors that significantly influence the process of interest. Furthermore, the study provides a critical examination of recent advancements and innovations in  $\text{CH}_4$  capture by ILs. ILs, in general, have a higher selectivity for methane compared to conventional solvents. This means that ILs can remove methane more effectively from VAM, resulting in a higher purity of the recovered methane. Overall, ILs offer several advantages over conventional solvents for the after treatment of VAM. They are more selective, less volatile, have a wider temperature range, are chemically stable, and can be made from renewable materials. As a result of their many advantages, ILs are becoming increasingly popular for the after treatment of VAM. They offer a more sustainable, efficient, and safe alternative to conventional solvents, and they are likely to continue gaining market share in the coming years.

**Keywords:** ionic liquid; absorption; methane; equation of state; Henry's law; ventilation air methane



**Citation:** Rahimpour, H.R.; Zanganeh, J.; Moghtaderi, B. Abatement of Greenhouse Gas Emissions from Ventilation Air Methane (VAM) Using Ionic Liquids: A Review of Experimental Methods and Modelling Approaches. *Processes* **2023**, *11*, 1496. <https://doi.org/10.3390/pr11051496>

Academic Editor: Xiaoyan Ji

Received: 5 April 2023

Revised: 5 May 2023

Accepted: 11 May 2023

Published: 15 May 2023



**Copyright:** © 2023 by the authors. Licensee MDPI, Basel, Switzerland. This article is an open access article distributed under the terms and conditions of the Creative Commons Attribution (CC BY) license (<https://creativecommons.org/licenses/by/4.0/>).

## 1. Introduction

Methane ( $\text{CH}_4$ ), as the principal component of natural gas, is an important Greenhouse Gas (GHG) and a substantial driver of global climate change. Emissions of  $\text{CH}_4$ , as the second most prevalent anthropogenic GHG, damages the ozone layer and accelerate environmental degradation.  $\text{CH}_4$  can trap heat up to 25 times more effectively than carbon dioxide ( $\text{CO}_2$ ), which directly contributes to global warming. Most of the  $\text{CH}_4$  emissions primarily come from specific sources targeted by the Global Methane Initiative (GMI): agriculture (including manure management, rice cultivation, and enteric fermentation), waste processing (such as wastewater and municipal solid waste), and industry and energy sectors (specifically, oil and natural gas systems, coal mines, biomass, and mobile and stationary combustion). Anthropogenic  $\text{CH}_4$  emissions are mainly released from the energy sector, with coal mining accounting for 22% of the total gas emissions [1–4].

$\text{CH}_4$  is emitted into the atmosphere at a wide range of concentrations. The  $\text{CH}_4$  concentration of different generating sources is classified into three categories: high purity,

medium purity, and dilute (<0.5%). High-purity CH<sub>4</sub> is desirable because common industrial processes can convert it to different chemicals (such as carbon black or methanol) or sell it to the natural gas market as a commodity. From the medium purity CH<sub>4</sub>, high-grade heat and electricity can be generated through a variety of fully developed technologies. In addition, small flows of medium purity CH<sub>4</sub> can simply be flared. It should be kept in mind that by using developed technologies (for instance, Thermal Flow-Reversal Reactor (TFRR)), only low-grade heat and an insignificant amount of electricity can be obtained. Concentrating dilute purity streams to medium purity CH<sub>4</sub> and medium purity to high purity CH<sub>4</sub> streams is highly desirable. CH<sub>4</sub> concentration is generally substantial in common purification processes because, at higher concentrations, non-methane components (such as H<sub>2</sub>S and CO<sub>2</sub>) are absorbed, but below concentration levels of 40%, special sorbents are needed to separate CH<sub>4</sub> [4].

On the other hand, Ventilation Air Methane (VAM) refers to the CH<sub>4</sub> that is released into the atmosphere during coal mining operations. During coal extraction from underground coal mines, ample fresh air must be constantly pumped into the mine to dilute the CH<sub>4</sub> concentration. This will also assist in maintaining oxygen concentration at a healthy level for the operators to breathe. As the fresh air moves through the mine, it picks up CH<sub>4</sub> that has been released by the coal deposits. Without proper ventilation, this CH<sub>4</sub> could build up to dangerous levels. The high CH<sub>4</sub> concentration in the presence of an ignition source with sufficient energy can ignite and lead to explosions. VAM technologies have been developed to capture the CH<sub>4</sub> that is present in the ventilation air and convert it into a usable energy source. This not only reduces the amount of greenhouse gases released into the atmosphere but also provides a potential revenue stream for the mining operations. The captured CH<sub>4</sub> can be used to power equipment or generate electricity, reducing the reliance on fossil fuels and lowering the carbon footprint of the mining industry.

Essentially, coal seams contain considerable quantities of CH<sub>4</sub>, and this leads to a safety hazard to miners, because at a specific concentration range (5 to 15% in air) it can be explosive. As stated earlier, to maintain safe working conditions, gassy underground coal mines use large-volume ventilation systems to remove CH<sub>4</sub> from the mine via dilution processes. Consequently, a CH<sub>4</sub> stream with a very dilute concentration is released into the atmosphere. Despite the low concentration (typically < 1%) of CH<sub>4</sub> in the VAM stream, due to the large VAM flow rates (~600 m<sup>3</sup>/s in a typical underground mine), the VAM emissions constitute more than 500 billion cubic feet of CH<sub>4</sub> per year. This CH<sub>4</sub> emission is equivalent to more than 300 million tons of CO<sub>2</sub> entering the atmosphere [5,6]. Simultaneously, CH<sub>4</sub> emissions, if harvested, can serve as a clean resource with considerable economic benefits and a large capacity for energy production. Progress in successful CH<sub>4</sub> utilisation and mitigation technologies would efficiently decline GHG emissions resulting from coal mining [4,7].

VAM includes CO<sub>2</sub>; oxygen (O<sub>2</sub>); nitrogen (N<sub>2</sub>); water vapor; CH<sub>4</sub>, coal dust; and particulates traces of H<sub>2</sub>, He, NO<sub>x</sub>, NH<sub>3</sub>, HCN, SO<sub>2</sub>, and H<sub>2</sub>S, and particles of CaCO<sub>3</sub> also exist. Characteristic information such as particle size, flow rate, the presence of other components, dust loading, and dust mineral matters of coal mine emissions is important in developing effective technologies for VAM mitigation and utilisation [7,8].

## 2. Methods for CH<sub>4</sub> Capture from VAM

### 2.1. Oxidation

Oxidation of very dilute CH<sub>4</sub> concentration has attracted significant attention to date because oxidation of CH<sub>4</sub> (conversion of CH<sub>4</sub> to CO<sub>2</sub>) can reduce its global warming potential by up to 95%. By oxidation, CH<sub>4</sub>, which is challenging for the absorption processes, is converted to CO<sub>2</sub>, which can be readily adsorbed from ventilation air with less GHG potential. Based on the mechanisms of kinetic combustion, CH<sub>4</sub> oxidation processes are classified as catalytic and thermal oxidation [3,7].

Thermal and catalytic oxidation are alternative methods for the capture of methane by initially converting it to carbon dioxide. In this process, CH<sub>4</sub> is burned in the presence of O<sub>2</sub> to form CO<sub>2</sub> and water (H<sub>2</sub>O).

Thermal oxidation involves burning the methane at high temperatures (typically 800 to 1000 °C) to initiate the chemical reaction. The process is typically carried out in a combustion chamber, where the methane is mixed with air or oxygen and ignited. Thermal oxidation is effective at converting methane to CO<sub>2</sub>, but it can be energy-intensive and produce high levels of nitrogen oxides (NO<sub>x</sub>) and other pollutants.

Catalytic oxidation, on the other hand, uses a catalyst to lower the temperature required for the reaction to occur. The catalyst typically consists of precious metals such as platinum, palladium, or rhodium, which promote the oxidation of methane to CO<sub>2</sub>. The process is carried out at lower temperatures (typically 200 to 500 °C), which reduces the energy required for the reaction and reduces the formation of pollutants.

Both thermal and catalytic oxidation can be effective at capturing methane, but they have their own advantages and disadvantages. Thermal oxidation is effective but energy-intensive, while catalytic oxidation is less energy-intensive but requires a costly catalyst. Additionally, both methods require careful management of the resulting CO<sub>2</sub> emissions to prevent environmental damage. Compared to absorption-based methods for capturing methane, thermal and catalytic oxidation have the advantage of not producing any waste streams that require disposal or treatment. However, they do require a significant amount of energy and may not be suitable for all applications. The choice of which method to use will depend on factors such as the scale of the operation, the availability of energy sources, and the cost-effectiveness of the process [3,9,10].

## 2.2. Clathrate Hydrate Formation

Gas clathrate hydrate formation, which encages small guest molecules such as CH<sub>4</sub> or CO<sub>2</sub> by a lattice of H-bonded water molecules, is another promising technique in carbon capturing from VAM. By converting CH<sub>4</sub> to hydrate form and maintaining other gases present in the gaseous form, separation of CH<sub>4</sub> takes place. Considering the lower hydrate formation pressure of CH<sub>4</sub> compared to other components at the same temperature value, CH<sub>4</sub> converts to the hydrate form earlier and is finally recovered purely after the decomposition of hydrates, resulting in its separation from the initial gas mixture. Nonetheless, some challenges are considerable in this approach, such as performance in streams with high flow rates of VAM and the existence of contaminants and coal dust in the inlet gas stream [7,11,12]. While it is true that the presence of other compounds could complicate the process of methane uptake using clathrate hydrates, several promoters have been studied to increase the selectivity towards methane separation [13–15].

## 2.3. Membrane

Gas separation by membranes is another remarkable method for CH<sub>4</sub> capturing from VAM. Polymeric membranes consisting of cellulose acetate, polyether block amide, polyamide, and silicone rubber have been widely studied for this purpose. Although these kinds of membranes are effective for the separation of CH<sub>4</sub> (and CO<sub>2</sub>), they are susceptible to damage from aggressive gases, their separation speed and the accumulation rate of gases are slow, and the method is expensive. Recently, Supported Ionic Liquid Membranes (SILMs) have attracted attentions due to their cost-effectiveness, favourable selectivity, insignificant vapour pressure, and high efficiencies [1,16,17].

## 2.4. Adsorption

The separation of methane using solid adsorbents is a promising technology for both natural gas purification and biogas upgrading. Solid adsorbents such as zeolites, Metal-Organic Frameworks (MOFs), and activated carbons can selectively adsorb methane from a gas mixture, allowing for the separation and purification of the gas. This technology is energy-efficient, environmentally friendly, and has the potential to significantly reduce

the cost of natural gas purification. However, the performance of the adsorbents is highly dependent on their intrinsic properties, such as pore size, surface area, and selectivity. Hence, further research is needed to optimise their performance and selectivity, and reduce the overall cost of the process [18–20].

### 2.5. Solvent Absorption

One of the most cost-effective techniques for the separation of hydrocarbons in the industry is solvent absorption. Chemical solvents (such as monoethanolamine (MEA)) and physical solvents (such as Selexol, Reticsol, and Purisol) are widely used in the natural gas industry. Some drawbacks of these solvents are their high solvent volatility, low selectivity/capacity, corrosivity, high energy required for the solvent regeneration, and economic and environmental limitations. In addition, conventional solvents are poor absorbers of CH<sub>4</sub>. Therefore, it is essential to design new adsorbents for the separation of light hydrocarbons. Recently, Ionic Liquids (ILs) have attracted much attention due to their specific properties [21–24].

## 3. Ionic Liquids

ILs, a novel generation of solvents, have unique properties such as large liquidus range, negligible vapor pressure, non-flammability, high chemical and thermal stability, high solvating capacity of inorganic and organic solutes, high ionic conductivity, low viscosity, low corrosion, and biodegradability. Therefore, ILs have shown promising potential as solvents in absorption-based processes for the capture of methane gas. However, there are several shortcomings of using ILs as solvents in this process, which include the high cost of ionic liquids, low solubility of methane in certain ionic liquids, high viscosity of ionic liquids, stability, and environmental concerns. The advantages and disadvantages of ILs are outlined compared to conventional organic solvent in Table 1. Despite these shortcomings, ionic liquids still have the potential to be a viable option for methane capture. Ongoing research is aimed at developing ionic liquids with improved solubility for methane, lower viscosity, and lower cost. If these challenges can be overcome, ionic liquids could become a promising alternative to traditional solvents for methane capture [25–28].

**Table 1.** Advantages and disadvantages of ionic liquids compared to conventional organic solvent [25–28].

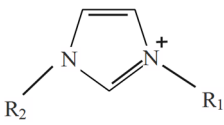
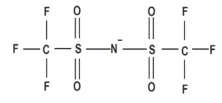
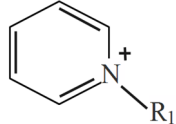
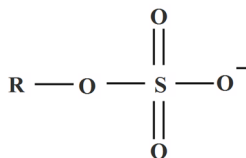
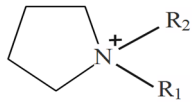
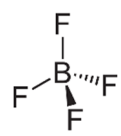
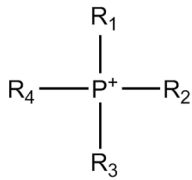
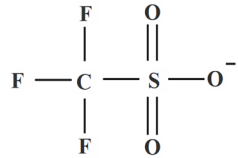
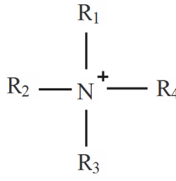
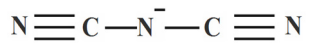
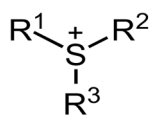
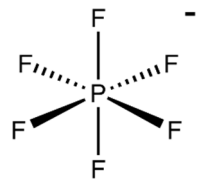
Aspect	Ionic Liquids	Conventional Organic Solvents
Solvent properties	High polarity and low volatility, good solvation power, tuneable properties	Variable polarity and volatility, limited solvation power, limited tunability
Environmental impact	Lower toxicity, non-flammable, low vapor pressure	Higher toxicity, flammable, high vapor pressure
Stability	High thermal and chemical stability, wide temperature range	Limited thermal and chemical stability, narrow temperature range
Reusability	Can be reused multiple times with minimal loss of performance	Limited reusability due to degradation and contamination
Cost	Generally more expensive than conventional solvents	Generally less expensive than ionic liquids
Accessibility	Limited availability of some types of ionic liquids	Wide availability of conventional solvents

As ILs consist of different sizes of organic or inorganic anions and asymmetric organic cations with a large size, they are tuneable to obtain desirable properties, which makes them designer solvents. In line with more efficient products and processes, ILs can be designed by an endless combination of anions and cations [16,24,29,30].

### 3.1. Constituent Ions

The ILs, as designer solvents, can be designed through the combination of constituent anions, cations, and functional groups for a specific application. The physical properties of ILs are generally controlled by cations, and the functionality and chemistry of ILs depend on anions. Despite the diversity of ILs, the most common are based on imidazolium, ammonium, pyridinium, pyrrolidinium, and phosphonium cations [31,32]. Table 2 illustrates the common cations and anions in ILs.

**Table 2.** Common cations and anions of ILs [33,34].

Name of Cation	Structure of Cation	Name of Anion	Structure of Anion
Imidazolium		Bis (trifluoromethylsulfonyl) imide	
Pyridinium		Alkyl sulphate	
Pyrrolidinium		Tetrafluoroborate	
Phosphonium		Triflate	
Ammonium		Dicyanamide	
Sulfonium		Hexafluorophosphate	

### 3.2. Ionic Liquid Media for CH<sub>4</sub> Capture

Although hydrocarbons have low solubility in many ILs, there are some specific kinds possessing long alkyl chains in their ion structures, which leads to their higher solvation capacity [35]. According to investigations that have been carried out so far, the most common ILs in use are those consisting of N-alkylpyridinium, alkylphosphonium, alkylammonium, and N,N-dialkylimidazolium cations. A large number of ILs

practically utilised are those with N,N-dialkylimidazolium cations, and it seems that 1-butyl-3-methylimidazolium [bmim]<sup>+</sup> is the most common one [32,34,36–38]. In addition, bis (trifluoromethylsulfonyl) imide [Tf<sub>2</sub>N], tetrafluoroborate [BF<sub>4</sub>], hexafluorophosphate [PF<sub>6</sub>], dicyanamide [DCA], methyl sulfate [MeSO<sub>4</sub>], methylphosphonate [MePO<sub>3</sub>], ethyl sulfate [EtSO<sub>4</sub>], tris(pentafluoroethyl)trifluorophosphate [FAP], tricyanomethanide [TCM], trifluoromethanesulfonate [CF<sub>3</sub>SO<sub>3</sub>], octylsulfate [OctSO<sub>4</sub>], nitrate [NO<sub>3</sub>], and bis(2,4,4-trimethylpentyl)phosphinate [TMPP] are the most common anions used for processes involving solvation purposes (Table 3).

**Table 3.** ILs commonly employed for CH<sub>4</sub> solubility.

ILs	Abbreviation	References
1-methyl-3-methylimidazolium methyl sulfate	[MMIM][MeSO <sub>4</sub> ]	[39]
1,3-dimethylimidazolium methylphosphonate	[C <sub>1</sub> -MIM][MePO <sub>3</sub> ]	[40]
1-Ethyl-3-methylimidazolium tetrafluoroborate	[EMIM][BF <sub>4</sub> ]	[39]
1-ethyl-3-methylimidazolium bis(trifluoromethylsulfonyl)imide	[EMIM][Tf <sub>2</sub> N]	[39]
1-Ethyl-3-methylimidazolium ethyl sulfate	[EMIM][EtSO <sub>4</sub> ]	[41]
1-ethyl-3-methylimidazolium tris(pentafluoroethyl)trifluorophosphate	[EMIM][FAP]	[42]
1-Ethyl-3-methylimidazolium tricyanomethanide	[EMIM][TCM]	[34]
1-Butyl-3-methylimidazolium hexafluorophosphate	[BMIM][PF <sub>6</sub> ]	[43]
1-butyl-3-methylimidazoliumtrifluoromethanesulfonate	[C <sub>4</sub> -MIM][CF <sub>3</sub> SO <sub>3</sub> ]	[40]
1-butyl-3-methylimidazolium octylsulfate	[C <sub>4</sub> -MIM][OctSO <sub>4</sub> ]	[40]
1-butyl-3-methylpyridinium tetrafluoroborate	[BMIM][BF <sub>4</sub> ]	[37]
1-butyl-3-methylimidazolium methyl sulfate	[BMIM][CH <sub>3</sub> SO <sub>4</sub> ]	[44]
1-butyl-3-methyl-imidazolium bis[(trifluoromethyl)sulfonyl]imide	[C <sub>4</sub> mim][Tf <sub>2</sub> N]	[36]
1-hexyl-3-methylimidazolium bis(trifluoromethylsulfonyl)imide	[HMIM][Tf <sub>2</sub> N]	[45]
1-Butyl-3-methylimidazolium nitrate	[HMIM][NO <sub>3</sub> ]	[24]
1-hexyl-3-methylimidazolium tricyanomethanide	[HMIM][TCM]	[46]
1-(2-hydroxyethyl)-3-methylimidazolium bis(trifluoromethanesulfonyl)imide	[C <sub>2</sub> OH-MIM][Tf <sub>2</sub> N]	[40]
1-n-hexyl-3-methylpyridinium bis(trifluoromethanesulfonyl)imide	[HMPY][Tf <sub>2</sub> N]	[32]
1-butyl-4-methylpyridinium tetrafluoroborate	[C <sub>4</sub> -mpy][BF <sub>4</sub> ]	[37]
trihexyltetradecylphosphonium bis(2,4,4-trimethylpentyl)phosphinate	[P <sub>(14)666</sub> ][TMPP]	[47]
trimethyl(hexyl)ammonium bis(trifluoromethylsulfonyl)imide	[N <sub>(6)111</sub> ][Tf <sub>2</sub> N]	[40]
1,1,3,3-tetramethylguanidium lactate (TMG) lactic acid (LAC)	[TMG][LAC]	[48]
1-Ethyl-3-methylimidazolium diethylphosphate	[EMIM][DEP]	[21]
1-Allyl-3-methylimidazolium dicyanamide	[AMIM][DCA]	[21]
Propionate N-methyl-(2-hydroxyethyl)amine	[m <sub>2</sub> HEA][Pr]	[49,50]
Propionate bis(2-hydroxyethyl)amine	[BHEA][Pr]	[49]
Propionate (2-hydroxyethyl)amine	[2HEA][Pr]	[49]
Bis(2-hydroxyethyl) ammonium butanoate	[BHEA][Bu]	[50]
Trihexyltetradecylphosphonium bis(2,4,4-trimethylpentyl) phosphinate	[thtdp][phos]	[21]
Trihexyltetradecylphosphonium dicyanamide	[thtdp][dca]	[21]
1-Butyl-1-methylpyrrolidinium dicyanamide	[bmpyrr][dca]	[21]
1,2,3-Tris(diethylamino)cyclopropenylium dicyanamide	[cprop][dca]	[21]

Table 3. Cont.

ILs	Abbreviation	References
1,2,3-Tris(diethylamino)cyclopropenylium bis(trifluoromethylsulfonyl)imide	[cprop][ Tf <sub>2</sub> N]	[21]
1-Butyl-1-methylpiperidinium bis(trifluoromethylsulfonyl)imide	[bmpip][ Tf <sub>2</sub> N]	[21]
Triethylsulfonium bis(trifluoromethylsulfonyl)imide	[TES][ Tf <sub>2</sub> N]	[21]
Methyltrioctylammonium bis(trifluoromethylsulfonyl)imide	[TOA][ Tf <sub>2</sub> N]	[21]
1-butyl-3-methylimidazolium methanesulfonate	[BMIM][ CF <sub>3</sub> SO <sub>3</sub> ]	[21]
1-methyl-3-methylimidazolium methyl sulfate	[MMIM][MeSO <sub>4</sub> ]	[40]

A large number of experimental and modelling investigations conducted on CO<sub>2</sub> absorption in ILs have revealed that the anion used has the highest effect on CO<sub>2</sub> solubility, and CO<sub>2</sub> is highly soluble in imidazolium-based ionic liquids. Experimentally, it has been discovered that the anion ([Tf<sub>2</sub>N<sup>−</sup>]) has the highest affection for CO<sub>2</sub> absorption [51]. Ultimately, 1-butyl-3-methylimidazolium bis(trifluoromethylsulfonyl) imide [bmim][Tf<sub>2</sub>N] has proved to be the best ionic liquid for CO<sub>2</sub> capture by most researchers [45,51–65]. The study conducted by Anthony et al. [54] on the solubilities of various gases in imidazolium-based ILs with a variety of anions including [BF<sub>4</sub>], [PF<sub>6</sub>], and [Tf<sub>2</sub>N] also proved that the anion has the most significant influence on CO<sub>2</sub> solubility level. The results indicated that the [Tf<sub>2</sub>N] anion enhances the solubilities of all gases in comparison with ILs consisting of [BF<sub>4</sub>] and [PF<sub>6</sub>], while the [BF<sub>4</sub>] anion has an insignificant impact on the gas' solubilities compared with [PF<sub>6</sub>]. Furthermore, replacing the imidazolium cation with pyrrolidinium or quaternary ammonium, all with the [Tf<sub>2</sub>N] anion, showed minor variation in gas solubilities. Although studies on CH<sub>4</sub> solubility in ILs are scarce, experimental comparison proved that there is a remarkable capacity for [bmim][Tf<sub>2</sub>N] to dissolve CH<sub>4</sub> [36]. Chen et al. [40] determined the solubility of CH<sub>4</sub>, carbon dioxide, and nitrous oxide gases in various ILs and evaluated the role of anion and cation in their solubility. In their investigations, the solubility of [bmim]<sup>+</sup>-based ILs and then [Tf<sub>2</sub>N]-based ILs were investigated respectively. The results depicted that, unlike CO<sub>2</sub> solubility in ILs, the cation change has a more significant effect on CH<sub>4</sub> solubility than anion change. Furthermore, it seems that the [Tf<sub>2</sub>N] anion plays the most significant role in CH<sub>4</sub> solubility because the solubility increases with the number of fluoroalkyl groups that exist in the anion.

According to Table 4, the solubility of CH<sub>4</sub> is higher in [bmim][Tf<sub>2</sub>N] compared to others. The higher solubility of CH<sub>4</sub> in the presence of imidazolium-based cations is due to the existence of large nonpolar alkyl-chains, which leads to interaction with nonpolar CH<sub>4</sub> molecules.

Ramdin et al. [66] reported the solubility of CO<sub>2</sub>, CH<sub>4</sub>, H<sub>2</sub>S, CO, H<sub>2</sub>, and N<sub>2</sub> in the [bmim][Tf<sub>2</sub>N] IL. At constant temperature ( $T = 333.15$  K) by variation of pressure, the solubility of the gases mentioned was investigated. The solubility trend of gases studied with [bmim][Tf<sub>2</sub>N] was H<sub>2</sub>S > CO<sub>2</sub> > CH<sub>4</sub> > CO > N<sub>2</sub> > H<sub>2</sub>. Solubility behaviour is affected by the polarity of gases so that molecules such as CO<sub>2</sub>, H<sub>2</sub>S, and C<sub>2</sub>H<sub>6</sub>, which have an electric quadrupole moment, present higher solubility. Although the solubility of H<sub>2</sub>S is triple that of CO<sub>2</sub>, syngas desulfurizes before the removal of CO<sub>2</sub>. The same trend was reported by others in the presence of different ILs. CO<sub>2</sub> is the most soluble gas, due to powerful interactions (Lewis acid-base [46]) between anion and CO<sub>2</sub> [35], which is followed by C<sub>2</sub>H<sub>6</sub> and then CH<sub>4</sub> (only Van der Waals interaction [46]). The solubility of N<sub>2</sub> is less than CH<sub>4</sub>, and H<sub>2</sub> is the least soluble one.

**Table 4.** Experimental data for CH<sub>4</sub> solubility in imidazolium-based ILs.

Abbreviation	T (K)	P (MPa)	Henry's Constant (MPa)	Solubility (Mole Fraction × 10 <sup>3</sup> )	References
[BMIM][PF <sub>6</sub> ]	283.31–343.08	0.0456–0.096	74.79–113.8	0.87–1.57	[43]
[BMIM][CF <sub>3</sub> SO <sub>3</sub> ]	294.15–312.75	0.05132–0.05482	45.84–127.33	0.431–1.12	[40]
[BMIM][OctSO <sub>4</sub> ]	300.85–313.25	0.05093–0.05329	42.31–155.1	0.343–1.204	[40]
[BMIM][BF <sub>4</sub> ]	283.05–343.09	0.046–0.097	79.41–221.6	0.45–1.25	[37]
[BMIM][CH <sub>3</sub> SO <sub>4</sub> ]	293.15–413.20	1.363–8.853	34.5–44.1	9.1–46.1	[44]
[BMIM][TF <sub>2</sub> N]	300.31–449.12	1.51–16.105		29.8–224.5	[36,66]
[HMIM][TF <sub>2</sub> N]	298.15–313.15	0.02–0.98	32.9–38	1.33–24.6	[32]
[HMIM][NO <sub>3</sub> ]	293.15–343.15	0.874–3.055	11.189–11.417	20.4–99.3	[24]
[EMIM][eFAP]	293.30–363.42	2.076–8.692	38.48–44.43	52–155	[46]
[EMIM][TF <sub>2</sub> N]	299.65–312.35	0.05021–0.05268	25.89–125.9	1.939–0.418	[40]
[MMIM][MePO <sub>3</sub> ]	298.15–312.95	0.05102–0.05394	58.16–206.3	0.261–0.877	[40]
[HMIM][TCM]	293.26–363.37	1.80–10.36	68.2–80	25–10	[46]
[EMIM][DEP]	303–363	1.685–9.441		20–76	[21]
[EMIM][FAP]	303–363	2.076–8.692	38.48–44.43	52–155	[42]
[C2OHmim][TF <sub>2</sub> N]	300.05–301.25	0.05039–0.05062	19.27–20.42	2.479–2.614	[40]
[EMIM][EtSO <sub>4</sub> ]	292.31–293.63	0.198–10.150		1.3–40.5	[41]
[AMIM][DCA]	303–363	3.351–9.59		15–34	[41]

### 3.3. Ionic Liquid Recycling in Absorption Processes

Ionic liquids can be easily regenerated to be used as a solvent recycle stream in the absorption-based processes for the capture of methane gas. The regeneration process typically involves separating the captured methane from the IL by reducing the pressure or increasing the temperature to release the gas. This is because ionic liquids are typically non-volatile and have a high thermal stability. This means that they can be easily heated to a high temperature to remove the methane gas that has been absorbed. The regenerated ionic liquid can then be cooled and reused in the absorption process.

There are several different methods that can be used to regenerate ionic liquids. One common method is to use a vacuum distillation process. In this process, the ionic liquid is heated under a vacuum, which causes the methane gas to vaporise. The vaporised methane gas is then removed from the system, leaving behind the regenerated ionic liquid. Another method that can be used to regenerate ionic liquids is to use a pressure swing absorption process. In this process, the ionic liquid is first compressed to a high pressure. This increases the solubility of the methane gas in the ionic liquid. The pressurised ionic liquid is then passed through a column where the methane gas is stripped out. The stripped methane gas is then released from the system, leaving behind the regenerated ionic liquid. The choice of regeneration method will depend on a number of factors, including the type of ionic liquid being used, the amount of methane gas that needs to be removed, and the desired purity of the regenerated ionic liquid [67–69].

## 4. Common Experimental Approaches

### Apparatus and Methods

The ILs prepared are generally impure, and the water content should be measured before and after solubility measurement due to the influence of impurity in thermophysical and thermodynamic properties. Karl Fisher titration is used to measure the water content at  $T = 343$  K for 15 h under vacuum. To check the conditions and the time for degassing and drying the ILs sample, several tests are performed. The solubility of gases in ILs are

measured according to the phase equilibrium that occurs in the Cialletet apparatus (as an Equilibrium Cell (EC) and high-pressure vessel). The experimental system for  $\text{CH}_4$  absorption is schematically illustrated in Figure 1 [36,37,40].

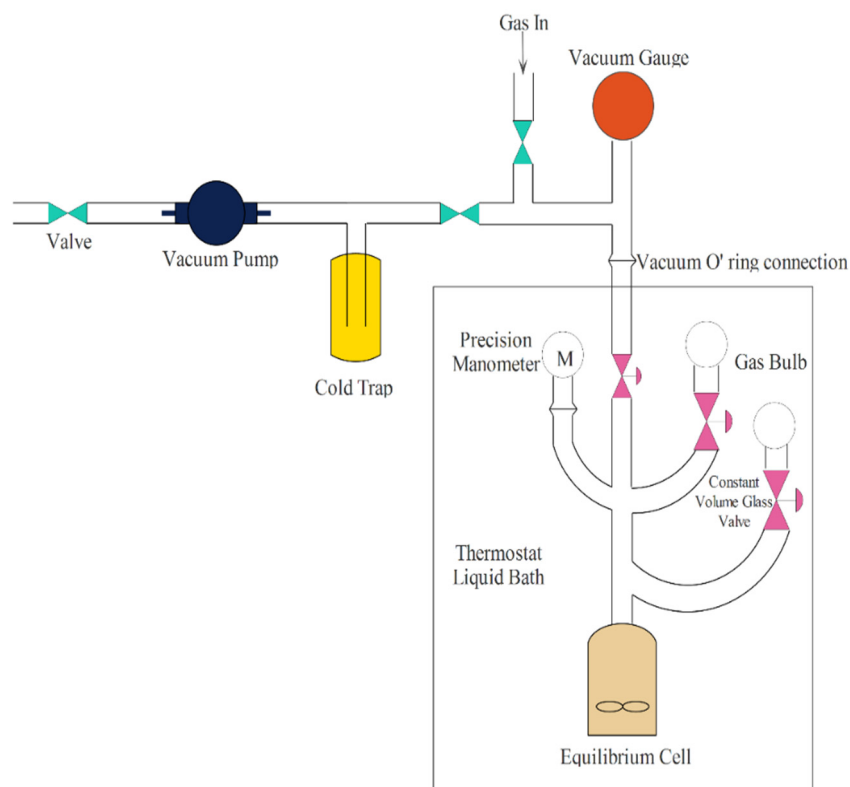


**Figure 1.** A schematic diagram of the  $\text{CH}_4$  solubility apparatus [37,40].

The preparation of the sample begins in a Pyrex tube containing the injected IL. A gas-rack is attached to the tube in order to degas the known amount of IL under vacuum, thus dosing the specific amount of gases present. Next, the binary mixture with specific composition at the tube exits from gas-rack and enters the Cialletet apparatus. To determine the injected feed gas composition at the initial pressure, the vapor phase is sampled instantly. By variation of pressure at constant temperature and fixed composition (until a phase-transition occurs and is observed visually (the last gas-bubble vanishes in the liquid phase)), the solubility of the desired gases is calculated in accordance with bubble point measurement. By utilization of a suitable equation of state, the mole amount of the desired gases can be calculated from the known volume, temperature, and pressure. Solubility results are presented in terms of Henry's law constants and solute mole fractions. It should be pointed out that the solubility of  $\text{CH}_4$  in the IL is investigated at various temperatures by simply changing the oven temperature and waiting for a new equilibrium state. As expected, it was observed that  $\text{CH}_4$  solubility in ILs enhances with rising pressure and reducing temperature. Nonetheless, at low temperatures, the temperature exerts a more noticeable effect on the solubility of  $\text{CH}_4$ . By increasing the temperature, this effect reduces significantly. More precisely, at high temperatures, the solubility of  $\text{CH}_4$  would not significantly increase by decreasing the temperature [36,43,46].

To sum up, to determine the solubility of  $\text{CH}_4$  in different ILs, a specific amount of  $\text{CH}_4$  is placed in contact with a known amount of IL at a constant temperature. At thermodynamic equilibrium, the pressure over the IL solution is constant and is related

directly to the CH<sub>4</sub> solubility in the IL (Figure 1). The solubility of CH<sub>4</sub> (2) in the IL (1) is determined in mole fraction from the following equations [37,40,43,60].

$$x_2 = \frac{n_2^{\text{IL}}}{n_1^{\text{IL}} + n_2^{\text{IL}}} \quad (1)$$

$$n_2^{\text{IL}} = n_{2,\text{initial}}^{\text{CH}_4} - n_{2,\text{equilibrium}}^{\text{CH}_4} \quad (2)$$

$$n_{2,\text{initial}}^{\text{CH}_4} = \frac{P_{\text{initial}} \cdot V_{\text{bulb}}}{Z_{(P_{\text{initial}}, T_{\text{initial}})} \cdot R \cdot T_{\text{initial}}} \quad (3)$$

$$n_{2,\text{equilibrium}}^{\text{CH}_4} = \frac{P_{\text{equilibrium}} \cdot (V_{\text{total}} - V_{\text{IL}} - V_{\text{mb}})}{Z_{(P_{\text{equilibrium}}, T_{\text{equilibrium}})} \cdot R \cdot T_{\text{equilibrium}}} \quad (4)$$

$$V_{\text{IL}} = \frac{m_{\text{initial}}}{\rho} \quad (5)$$

The symbols are listed in Table 5.

**Table 5.** List of symbols used in the solubility equations, Equations (1)–(5).

Symbol	Name
$n_2^{\text{IL}}$	The amount of gaseous solute (CH <sub>4</sub> ) dissolved in the IL
$n_1^{\text{IL}}$	$n_1^{\text{IL}} = n_1^{\text{total}}$ is the entire amount of IL calculated by weighing
$n_{2,\text{initial}}^{\text{CH}_4}$	The quantity of CH <sub>4</sub> initially present in the bulb of glass
$n_{2,\text{equilibrium}}^{\text{CH}_4}$	The quantity of CH <sub>4</sub> in equilibrium with the IL
$P_{\text{initial}}$	The initial pressure of CH <sub>4</sub> present in the gas bulb
$V_{\text{bulb}}$	The volume of the bulb initially filled with CH <sub>4</sub>
$T_{\text{initial}}$	The initial temperature of CH <sub>4</sub> present in the gas bulb
$R$	The universal gas constant
$Z$	The compressibility factor for the pure CH <sub>4</sub> ; it is assumed as an ideal gas, therefore $Z = 1$
$P_{\text{equilibrium}}$	Equilibrium pressure
$V_{\text{total}}$	The total volume of the equilibrium cell
$V_{\text{IL}}$	The volume occupied by the IL at $T_{\text{equilibrium}}$ and $P_{\text{equilibrium}}$
$V_{\text{mb}}$	The volume of the magnetic bar
$T_{\text{equilibrium}}$	Equilibrium Temperature
$m_{\text{initial}}$	The initial quantity of the IL
$\rho$	The density of the IL

## 5. Process Modelling

The experimental disadvantages for the determination of CH<sub>4</sub> solubility along with lengthy experimental processes as well as high-priced operations are the principal reasons for providing computational methods and thermodynamic approaches to determine the interactions and phase equilibrium of CH<sub>4</sub> in different ionic liquids. Furthermore, identifying the operating conditions to access the actual solubilities for ionic liquids is essential to effectively and efficiently design the systems employing the various gas mixtures with ILs.

### 5.1. Thermodynamic Properties of Solvation

The solubility of gases, expressed by Henry's law constant, is influenced by temperature variation. In fact, the gases' solubility corresponds to the thermodynamic properties

of the solution. These properties give important information regarding the enthalpy of the solution (related to interactions between solvent and solute) and the entropy of the solution (solution's molecular structure). Solubility variation by temperature is not similar for different gases. Except for O<sub>2</sub> and CO (almost constant solubility) and H<sub>2</sub> (close to zero enthalpy), all the gases presented negative solution enthalpies, indicating an exothermic solvation. Therefore, the solubility of CH<sub>4</sub> decreases with temperature [37,42,43]. In addition, the solubility of CH<sub>4</sub> increases significantly with pressure increase, and the influence of temperature variation is negligible [16,70].

## 5.2. Henry's Law

As the experimental data of CH<sub>4</sub> solubility in ILs has proved, the IL with the highest solubility has the lowest Henry's law constant. The constant of Henry's law ( $k_{H_{2,1}}$ ) for components with subscript 2 dissolved in a solvent with subscript 1 that depends on the temperature ( $T$ ) and pressure ( $P$ ) is determined by the following equation [40]:

$$k_{H_{2,1}} = \lim_{x_2 \rightarrow 0} \left[ \frac{f_2(T, P, x)}{x_2} \right] = f_{2,\text{pure liquid}}(T, P) \cdot \gamma_2^\infty \quad (6)$$

In classical thermodynamics, the relation of vapor–liquid equilibrium is written as:

$$f_{i,\text{pure liquid}} \cdot \gamma_i = \frac{p \cdot y_i \cdot \varphi_i^{\text{vapor}}(T, P, y)}{x_i} \quad (7)$$

Therefore, the previous equation for the solute gas (component 2) would be:

$$f_{2,\text{pure liquid}} \cdot \gamma_2 = \frac{p \cdot y_2 \cdot \varphi_2^{\text{vapor}}(T, P, y)}{x_2} \quad (8)$$

In low pressure  $\varphi_2^{\text{vapor}}(T, P, y) = 1$  and because there is no solvent (IL) in the gas phase  $y_2 = 1$ , and finally:

$$k_{H_{2,1}} = \frac{P_{\text{Equilibrium}}}{x_i} \quad (9)$$

The constants of Henry's law are converted exactly to the Gibbs energy of solvation, based on Equation (10) [37]. At a constant temperature, the partial molar Gibbs energy changes when the solute is moved from the pure ideal gas state to the state of infinite dilution of the solute in the solvent at the standard pressure. At low pressures, when the solutes are in gaseous state, the free energy of solvation is a great estimation for the Gibbs energy of the solution.

$$\Delta_{\text{solvation}} G^\infty = R \cdot T \cdot \ln\left(\frac{K_H}{p^\circ}\right) \quad (10)$$

Considering the temperature and computing the partial derivatives of the Gibbs energy, the partial molar differences in enthalpy (Equation (11)) and entropy (Equation (12)) between the two states are achieved as follows:

$$\Delta_{\text{solvation}} H^\infty = -T^2 \cdot \frac{\partial}{\partial T} \left( \frac{\Delta_{\text{solvation}} G^\infty}{T} \right) = -R \cdot T^2 \cdot \frac{\partial}{\partial T} \left( \ln\left(\frac{K_H}{p^\circ}\right) \right) \quad (11)$$

$$\Delta_{\text{solvation}} S^\infty = \frac{(\Delta_{\text{solvation}} H^\infty - \Delta_{\text{solvation}} G^\infty)}{T} = -R \cdot T \cdot \frac{\partial}{\partial T} \left( \ln\left(\frac{K_H}{p^\circ}\right) \right) - R \cdot \ln\left(\frac{K_H}{p^\circ}\right) \quad (12)$$

By applying group contribution equations, the Henry's law constant of gases in different ILs can be estimated. By correlating the constant of Henry's law as a function of

temperature by the following empirical equations, the representative solubility values can be calculated at the atmospheric pressure [37,40].

$$\ln \frac{K_H(T)}{10^5(Pa)} = \sum_{i=0}^n A_i \cdot \left(\frac{T}{K}\right)^{-i} \quad (13)$$

By considering  $n = 1$ , Henry's law constant is represented by the following equation:

$$\ln \frac{K_{H_{CH_4,IL}}(T)}{10^5(Pa)} = A_0 + \frac{A_1}{T} \quad (14)$$

Having known the molecular structure of the proposed ILs,  $A_0$  and  $A_1$  parameters are determined by group contributions as follow:

$$A_0 = \sum_i n_i \cdot G_i \quad (15)$$

$$A_1 = \sum_i n_i \cdot G'_i \quad (16)$$

Based on the investigations of Chen et al. [40], every proposed IL is defined by several groups; considering each anion and cation as a basic group, alkyl chains in cation or anion are broken into  $-CH_3$  and  $-CH_2-$ . The symbols used in the Henry's law equations are listed in Table 6. The authors gathered a large number of ILs with several experimental Henry's law constants and defined 19 basic groups, as listed in Table 7.

**Table 6.** List of symbols used in the Henry's law equation.

Symbol	Name
$f_2$	The fugacity of gas (CH <sub>4</sub> )
subscript 1	Solvent (IL)
subscript 2	Component (gas) dissolved in the solvent (IL)
$\gamma_2^\infty$	The activity coefficient of component (gas) 2 at infinite dilution
$k_{H_{2,1}}$	The constant of Henry's law
$x_2$	The mole fraction of Component (gas) dissolved in the solvent (IL)
$p^\circ$	The standard state of the pressure
$n_i$	Number of groups
$G_i$	Group Parameter
$G'_i$	Group Parameter

**Table 7.** Group Parameters ( $G_i$  and  $G'_i$ ) to calculate  $A_0$  and  $A_1$  [40].

Group	$G_i$	$G'_i$
CH <sub>2</sub>	1.695	−488.423
CH <sub>3</sub>	−0.145	35.661
Imidazolium	1.925	−512.809
Pyrilium	0.671	−168.551
Pyrridilium	1.491	−368.296
Ammonium	−0.697	232.171
Phosphonium	0.917	−57.890
Tetrafluoroborate	5.115	−403.870

Table 7. Cont.

Group	$G_i$	$G'_i$
Texafluorophosphate	4.648	−274.631
Phosphonate	0.900	91.800
Phosphate	4.107	98.388
Sulfonate	3.586	22.398
Sulfate	3.945	−136.707
Bis(perfluoromethylsulfonyl)imide	3.619	−110.162
Bis((trifluoromethyl)sulfonyl)imide	3.807	−160.684
Methoxy	−2.412	157.887
Hydroxy	1.041	−229.363
Trifluoromethane	−0.589	50.367
Bisfluoromethane	0.079	13.715

### 5.3. Thermodynamic Equation of State (EoS)

There have been a large number of efforts to model or correlate the solubilities of CH<sub>4</sub> in ILs. They are presented in this review paper in detail as follows:

#### 5.3.1. Extended Henry's Law Model (Extended Pitzer's Model)

Because the vapor pressure of ILs is neglected and assuming CH<sub>4</sub> to be a completely pure-gas phase, the Vapor–Liquid Equilibrium (VLE) state is applied just for the gas component. Therefore, the extended Henry's law is defined as follows [24,44,71–76]:

$$K_{H,CH_4}(T, P) \cdot a_{CH_4}(T, m_{CH_4}) = f_{CH_4}(T, P) \quad (17)$$

The effect of pressure on Henry's constant is represented as:

$$K_{H,CH_4}(T, P) = K_{H,CH_4}^{(0)}(T) \cdot \exp\left(\frac{PV_{m,CH_4}^{(\infty)}}{RT}\right) \quad (18)$$

The activity of CH<sub>4</sub> in the IL at temperature  $T$  (considering the negligible effect of pressure on the activity) is:

$$a_{CH_4} = \frac{m_{CH_4}}{m^\circ} \cdot \gamma_{CH_4} \quad (19)$$

In addition, the activity coefficient of CH<sub>4</sub> is determined by applying the virial expansion for the excess Gibbs energy on the molality scale as follows:

$$\ln \gamma_{CH_4} = 2 \cdot \left(\frac{m_{CH_4}}{m^\circ}\right) \cdot \beta_{(CH_4, CH_4)}^{(0)} + 3 \cdot \left(\frac{m_{CH_4}}{m^\circ}\right)^2 \cdot \mu_{(CH_4, CH_4, CH_4)} \quad (20)$$

Finally, the fugacity of CH<sub>4</sub> at equilibrium temperature and pressure is:

$$f_{CH_4}(T, P) = p \cdot \phi_{CH_4}(T, P) \quad (21)$$

Kumelan et al. [71] extrapolated the experimental data of the solubility of CH<sub>4</sub> in [hmim][Tf<sub>2</sub>N] at a constant temperature, determined Henry's constant at zero pressure, and estimated the relative uncertainty for the values of those Henry's constants, CH<sub>4</sub> partial molar volume at infinite dilution in [hmim][Tf<sub>2</sub>N], and binary and ternary interactions as follows:

$$K_{H,CH_4}^{(0)}(T) = \lim_{P \rightarrow 0} \left[ \frac{f_{CH_4}(T, P)}{\frac{m_{CH_4}}{m^\circ}} \right] \quad (22)$$

$$\ln(K_{H,CH_4}^{(0)}/\text{MPa}) = 6.4929 - \frac{835.9}{(T/\text{K})} - 0.003471 \cdot (T/\text{K}) \quad (23)$$

$$V_{m,CH_4}^{(\infty)} / (\text{cm}^3 \text{mol}^{-1}) = -5.4 + 0.029 \cdot (T/\text{K}) \quad (24)$$

$$\beta_{(CH_4,CH_4)}^{(0)} = 0 \quad (25)$$

$$\mu_{(CH_4,CH_4,CH_4)} = 0 \quad (26)$$

The symbols used in the extended Henry's law model (extended Pitzer's model) equations are listed in Table 8.

**Table 8.** List of symbols used in extended Henry's law (extended Pitzer's model) equation.

Symbol	Name
$f_{CH_4}(T, P)$	The fugacity of CH <sub>4</sub> in the vapor phase at temperature $T$ and pressure $P$
$a_{CH_4}(T, m_{CH_4})$	The activity of CH <sub>4</sub> in the IL at temperature $T$ (considering the negligible effect of pressure on the activity)
$K_{H,CH_4}(T, P)$	The constant of Henry's law of CH <sub>4</sub> in ILs at temperature $T$ and pressure $P$ on the molality scale
$K_{H,CH_4}^{(0)}(T)$	The constant of Henry's law of CH <sub>4</sub> in ILs at zero pressure
$V_{m,CH_4}^{(\infty)}$	Methane partial molar volume at infinite dilution in IL
$R$	The universal gas constant
$m^\circ$	=1 mol/kg
$\gamma_{CH_4}$	Activity Coefficient
$\beta_{(CH_4,CH_4)}^{(0)}$	Binary interaction between CH <sub>4</sub> molecules in the IL
$\mu_{(CH_4,CH_4,CH_4)}$	Ternary interaction between CH <sub>4</sub> molecules in the IL
$\phi_{CH_4}(T, P)$	Fugacity coefficient calculated with thermodynamic models [77]
$p$	Total pressure

### 5.3.2. The Peng–Robinson (PR) Equation of State

The experimental data of CH<sub>4</sub> + IL can be correlated using the Peng–Robinson Equation of State (PR-EoS) as follows [78–83]:

$$P = \left[ \frac{R \cdot T}{(V - b)} \right] - \left[ \frac{a(T)}{(V \cdot (V + b) + b \cdot (V - b))} \right] \quad (27)$$

The mixture parameters of ionic liquid are determined from the following mixing rules:

$$a = \sum_i \sum_j x_i \cdot x_j \cdot a_{ij} \quad (28)$$

$$a_{ij} = \sqrt{a_{ii} \cdot a_{jj}} \cdot (1 - k_{ij}) \quad (29)$$

$$b = \sum_i \sum_j x_i \cdot x_j \cdot b_{ij} \quad (30)$$

$$b_{ij} = \left[ \frac{1}{2} \cdot (b_i + b_j) \right] \cdot (1 - l_{ij}) \quad (31)$$

In which  $b_{ii} = b_i, b_{jj} = b_j$

$$a_{ii} = 0.457235 \cdot \frac{R^2 \cdot T_{ci}^2}{P_{ci}} \cdot \left[ 1 + \left( 1 - \left( \frac{T}{T_{ci}} \right)^{\frac{1}{2}} \right) \cdot (0.37464 + 1.54226 \cdot \omega_i - 0.26992 \cdot \omega_i^2) \right]^2 \quad (32)$$

$$b_i = 0.0077796 \cdot \frac{R \cdot T_{ci}}{P_{ci}} \quad (33)$$

To calculate the PR-EoS input parameters, the critical pressure ( $P_C$ ), critical temperature ( $T_C$ ), and the acentric factors ( $\omega$ ) of  $\text{CH}_4$  and ionic liquid are essential. Those characteristic properties of  $\text{CH}_4$  could be collected from the literature ( $M = 16.04 \text{ gmol}^{-1}$ ;  $T_C = 190.6 \text{ K}$ ;  $P_C = 4.599 \text{ MPa}$ ;  $\omega = 0.012$ ) [46,84]; nonetheless, those of ionic liquids are unavailable because most of the them are decomposed before reaching the critical point. Consequently, the critical pressure and temperature, along with other properties of ionic liquids, ought to be estimated with different methods such as molecular simulations or the group contribution method of modified Lydersen–Joback–Reid, which offers approximately good results, particularly for molecules with high molecular weights [79,80,82].

Based on the group contribution method of modified Lydersen–Joback–Reid for the parameters of interest we have:

$$T_b(\text{K}) = 198.2 + \sum n \cdot \Delta T_{bM} \quad (34)$$

$$T_C(\text{K}) = \frac{T_b}{\left[ 0.5703 + 1.0121 \cdot \sum n \cdot \Delta T_M - (\sum n \cdot \Delta T_M)^2 \right]} \quad (35)$$

$$P_C(\text{MPa}) : P_C(\text{bar}) = \frac{M}{\left[ 0.2573 + \sum n \cdot \Delta P_M \right]^2} \quad (36)$$

The acentric factor is determined by:

$$\omega = \frac{(T_C - 43) \cdot (T_b - 43)}{(0.7T_C - 43) \cdot (T_C - T_b)} \cdot \log \left[ \frac{P_C}{P_b} \right] - \frac{T_C - 43}{T_C - T_b} \cdot \log \left[ \frac{P_C}{P_b} \right] + \log \left[ \frac{P_C}{P_b} \right] - 1 \quad (37)$$

The acentric factor is measured from the normal boiling temperature and critical properties ( $T_b$  relates to  $P_b = 0.1 \text{ MPa}$ ). The symbols used in the Peng–Robinson (PR) equation of state are listed in Table 9.

**Table 9.** List of symbols used in the Peng–Robinson (PR) Equation of State (EoS).

Symbol	Name
$l_{ij}$	The binary interaction parameter and $l_{ij} = 0$
$k_{ij}$	The binary interaction parameter and $k_{ij} = 0$
$P_C$	Critical pressure
$T_C$	Critical temperature
$\omega$	Acentric factors
$M$	Molecular weight in ILs

The critical properties of approximately 300 ILs, as well as their acentric factors estimated utilizing the modified Lydersen–Joback–Reid method, were presented in the investigation conducted by Valderrama and Rojas [80].

Based on the literature, imidazolium-based ionic liquids proved to be an excellent candidate for  $\text{CH}_4$  absorption due to their lower surface tension and molar density. Therefore, Table A1 lists the critical properties of imidazolium-based ionic liquids (including 30 different types of anions) estimated from the modified Lydersen–Joback–Reid method.

### 5.3.3. Krichevsky–Kasarnovsky (KK) Equation

The equation of Krichevsky–Kasarnovsky has been applied extensively to describe the solubility of poorly soluble gases in ionic liquids up to extremely high pressures, as follows [73,85,86]:

$$\ln \frac{f_i(T, P)}{x_i} = \ln H_{h,x_i}^{P^S}(T) + \frac{V_i^\infty \cdot (P - P^S)}{RT} \quad (38)$$

Because the vapor pressure of the ionic liquids is negligible and approximately takes a zero value,  $P^S$  (saturated vapor pressure) is considered to be zero in Equation (38). Therefore, Equation (38) can then be written as Equation (39):

$$\ln \frac{f_i^0(T, P)}{x_i} = \ln H_{h,x_i}^{(0)}(T) + \frac{V_i^\infty \cdot P}{R \cdot T} \quad (39)$$

$H_{h,x_i}^{(0)}(T)$  and  $V_i^\infty$  at each temperature are measured from the intercept and slope of the plot of  $\ln \frac{f_i^0}{x_i}$  versus  $P$  for binary  $\text{CH}_4/\text{IL}$  mixtures, respectively.

The symbols used in the Krichevsky–Kasarnovsky (KK) equations are listed in Table 10.

**Table 10.** List of symbols used in Krichevsky–Kasarnovsky (KK) equations.

Symbol	Name
$f_i^0(T, P)$	The fugacity of pure $\text{CH}_4$ in the gas phase at pressure $P$ and temperature $T$
Subscript $i$	Represents Solute
$x_i$	The mole fraction of solute $i$ present in the solvent
$H_{h,x_i}^{P^S}(T)$	The constant of Henry's law for solute $i$ in the solvent on the mole-fraction scale and at the vapor pressure ( $P^S$ ) of IL solvent
$V_i^\infty$	The partial molar volume of gas solute $i$ at infinite dilution
$R$	The universal gas constant

Althuluth et al. [46] used the Krichevsky–Kasarnovsky equation to determine Henry's law constants for  $\text{CH}_4$  solubility in 1-hexyl-3-methylimidazolium tricyanomethanide [hmim][TCM]. The fugacity of pure  $\text{CH}_4$  in the gas phase was evaluated with the PR-EoS at each specific temperature, and the data were then calculated and presented as a plot of  $\ln \frac{f_i^0}{x_i}$  versus  $P$ , hence the slope gives  $\ln H_{h,x_i}^{(0)}$  (logarithm of Henry's law constant of  $\text{CH}_4$  in the solvent).

Althuluth et al. [42] calculated the solubility of  $\text{CH}_4$  in 1-Ethyl-3-methylimidazolium Tris (pentafluoroethyl) trifluorophosphate [emim][FAP] using Henry's constants and applying the Krichevsky–Kasarnovsky equation. They compared the results with the solubility of  $\text{CO}_2$  in the same IL to estimate the selectivity in the separation process. As Table 11 clearly illustrates, [emim][FAP] is a good candidate for sweetening natural gas because it integrates a high absorption capacity for  $\text{CO}_2$  (low Henry's constants) with a low solubility for  $\text{CH}_4$  (high Henry's constants), resulting in a high selectivity for  $\text{CO}_2$  over  $\text{CH}_4$  ( $S_{\text{CO}_2/\text{CH}_4} = \frac{H_{\text{CH}_4}}{H_{\text{CO}_2}}$ ) from 5.77 to 11.58, depending on the operating conditions. The maximum selectivity was obtained at the lowest temperatures.

It should be noted that classical thermodynamics explains the selectivity of the absorption process through the concept of partial pressure equilibrium. According to Henry's law (Section 5.2), the amount of gas that dissolves in a liquid at a given temperature is proportional to the partial pressure of each constituent of the gaseous mixture above the liquid. The proportionality constant is known as the Henry's law constant, which is specific to a particular gas-solvent system. When a gaseous mixture containing different compounds is brought into contact with a liquid solvent, the solubility of each molecule in the solvent de-

depends on its partial pressure in the mixture, or in other words its Henry's law constant. At equilibrium, the chemical potential of the compounds in the liquid phase and the gaseous mixture become equal, and the solubility of each individual gas is determined by its partial pressure in the gas mixture. Therefore, the selectivity of solutes for gas absorption depends on the differences in their partial pressures in the gaseous mixture and their respective Henry's law constants. If a gas has a higher partial pressure and, as a result, a higher Henry's law constant, it will be more readily absorbed by the solvent, whereas a gas with a lower partial pressure and consequently a lower Henry's law constant will be absorbed less readily. In summary, classical thermodynamics explains the selectivity of solutes for gas absorption in terms of partial pressure equilibrium, where the solubility of each gas in a liquid solvent depends on its partial pressure and Henry's law constant [87,88].

**Table 11.** The constant of Henry for the solubility of CH<sub>4</sub> and CO<sub>2</sub> in [emim][FAP] and calculated selectivities at different temperatures [42].

T (K)	$H_{CH_4}$ (MPa)	$H_{CO_2}$ (MPa)	$S_{\frac{CO_2}{CH_4}} = \frac{H_{CH_4}}{H_{CO_2}}$
303	38.48	3.32	11.58
313	39.48	4.05	9.74
323	40.47	4.67	8.65
333	41.46	5.35	7.74
343	42.45	6.08	6.98
353	43.44	6.86	6.33
363	44.43	7.70	5.77

#### 5.4. Artificial Intelligence Approaches

Thermodynamic equations of state, activity coefficient models, group contribution methods, the extended Pitzer's model, and other recommended models necessitate adjustable parameters that must be optimized based on experimental data, without which most of the suggested models cannot be completely reliable. In this regard, the neural network method is a flexible procedure which has been applied in order to model as well as predict the solubility and phase equilibrium of CH<sub>4</sub> in various ILs [89–95]. The neural network is an extensively used numerical technique that can model and predict every kind of data and information, even ranging from simple to complex. The method consists of different neurons located in the input layer, the hidden layer(s), and the output layer, as shown in Figure 2 [96]. The neurons are connected to the other ones placed in the next and previous layers. Each one has an input value which is processed by utilizing a transfer function to produce the output, as defined mathematically in Equation (40).

$$y_i = F(S_i) \quad (40)$$

By employing the hyperbolic tangent transfer function for neurons of the hidden layer, and using the linear transfer function for the output neuron, the input of each next-level neuron is determined based on the output of previous layers by the following equation [96]:

$$S_i = \sum_j w_{ji} \cdot y_j + b_i \quad (41)$$

The symbols used in artificial neural network equations are listed in Table 12. Propagation models are used to optimize biases and weights. In this regard, the Levenberg–Marquardt back propagation technique is commonly applied to train the network.

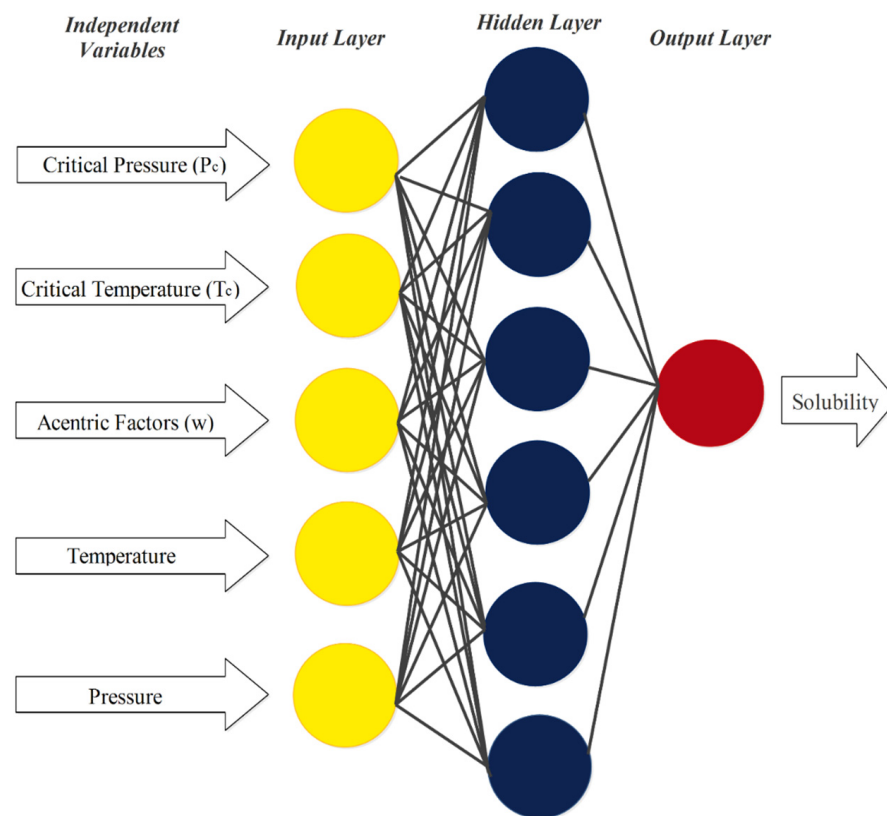


**Figure 2.** A schematic diagram of artificial neural network for prediction of CH<sub>4</sub> solubilities in ILs [96].

**Table 12.** List of symbols used in artificial network equations.

Symbol	Name
$y_i$	The output of $i$ -th neuron
$F$	The transfer function
$S_i$	The input of $i$ -th neuron
$y_j$	The output of the previous layer
$w_{ji}$	Weights relating $j$ -th neuron (from the previous layer) to $i$ -th neuron
$b_i$	The bias of $i$ -th neuron

## 6. Novel Approaches to Capture CH<sub>4</sub> Using ILs

The interest in CH<sub>4</sub> solubility in ILs has grown rapidly in recent years. Table 13 lists several recent papers centred on the capture of CH<sub>4</sub> using ILs.

**Table 13.** List of published papers focusing on CH<sub>4</sub> capture using ILs.

Highlights	ILs Used in the Study	Results	References
<ul style="list-style-type: none"> <li>Two hybrid artificial intelligent models, namely CSA-LSSVM and PSO-ANFIS, were developed to predict the solubility of CH<sub>4</sub> in ILS and correlate the inputs (temperature, critical pressure, acentric factor, and critical temperature of ILs) and outputs (bubble-point pressures of CH<sub>4</sub>).</li> </ul>	<ul style="list-style-type: none"> <li>Trihexyltetradecylphosphonium bis (2,4,4 trimethylpentyl) phosphinate [thtdp] [phos]</li> <li>1-ethyl-3-methylimidazolium diethylphosphate [emim][dep]</li> <li>Trihexyltetradecylphosphonium dicyanamide [thtdp][dca]</li> <li>1-butyl-1-methyl pyrrolidinium dicyanamide [bmpyrr][dca]</li> <li>1-allyl-3-methylimidazolium dicyanamide [amim][dca]</li> <li>1,2,3-tris(diethylamino)-cyclopropenylium dicyanamide [cprop][dca]</li> <li>1-butyl-1-methylpiperidinium bis(trifluoromethylsulfonyl)imide [bmpip][Tf<sub>2</sub>N]</li> <li>1,2,3-tris (diethylamino) cyclopropenyliumbis-(trifluoromethyl sulfonyl)imide [cprop][Tf<sub>2</sub>N]</li> <li>Methyl tri octylammonium bis-(trifluoromethylsulfonyl) imide[toa][Tf<sub>2</sub>N]</li> <li>Triethylsulfonium bis (trifluoromethylsulfonyl) imide [tes][Tf<sub>2</sub>N]</li> <li>1-Butyl-3-methylimidazolium bis(trifluoromethylsulfonyl) imide[bmim][Tf<sub>2</sub>N]</li> </ul>	<ul style="list-style-type: none"> <li>The results proved that artificial intelligence-based models are influential and favourable replacements for time-consuming and complicated investigational methods for predicting gas solubility.</li> </ul>	[97]
<ul style="list-style-type: none"> <li>The phase equilibria of CH<sub>4</sub> and various ILs were investigated.</li> <li>Two statistical EoSs, namely cubic-plus-association and modified Sanchez and Lacombe, were developed to estimate the solubility of CH<sub>4</sub> in different ILs using density data of ILs to calculate EoSs parameters.</li> </ul>	<ul style="list-style-type: none"> <li>1-Hexyl-3-methylimidazolium tricyanomethanide [hmim][TCM]</li> <li>Propionate N-methyl-(2-hydroxyethyl)amine [m2HEA][Pr]</li> <li>Propionate bis(2-hydroxyethyl)amine [BHEA][Pr]</li> <li>Propionate (2-hydroxyethyl)amine [2HEA][Pr]</li> <li>Bis(2-hydroxyethyl) ammonium butanoate [BHEA][Bu]</li> <li>1-Butyl-3-methylimidazolium bis(trifluoromethylsulfonyl) imide[bmim][Tf<sub>2</sub>N]</li> <li>1-Hexyl-3-methylimidazolium nitrate [Hmim][NO<sub>3</sub>]</li> <li>1-Ethyl-3-methylimidazolium diethylphosphate [emim][dep]</li> <li>Trihexyltetradecylphosphonium bis(2,4,4-trimethylpentyl) phosphinate [thtdp][phos]</li> <li>Trihexyltetradecylphosphonium dicyanamide [thtdp][dca]</li> <li>1-Allyl-3-methylimidazolium dicyanamide [amim][dca]</li> <li>1-Butyl-1-methylpyrrolidinium dicyanamide [bmpyrr][dca]</li> <li>1,2,3-Tris(diethylamino)cyclopropenylium dicyanamide [cprop][dca]</li> <li>1,2,3-Tris(diethylamino)cyclopropenylium bis (trifluoromethylsulfonyl)imide [cprop][Tf<sub>2</sub>N]</li> <li>1-Butyl-1-methylpiperidinium bis(trifluoromethylsulfonyl) imide [bmpip][Tf<sub>2</sub>N]</li> <li>Triethylsulfonium bis(trifluoromethylsulfonyl)imide [tes][Tf<sub>2</sub>N]</li> <li>Methyltrioctylammonium bis(trifluoromethylsulfonyl) imide [toa][Tf<sub>2</sub>N]</li> <li>1-Hexyl-3-methylpyridinium bis(trifluoromethylsulfonyl) imide [hmpy][Tf<sub>2</sub>N]</li> <li>1-hexyl-3-methylimidazolium bis(trifluoromethylsulfonyl)imide [hmim][Tf<sub>2</sub>N]</li> </ul>	<ul style="list-style-type: none"> <li>EoSs gave acceptable results and indicated that the correlative capacity of the proposed EoSs presents low Average Absolute Relative Deviations (AARDs).</li> </ul>	[98]

Table 13. Cont.

Highlights	ILs Used in the Study	Results	References
<ul style="list-style-type: none"> <li>High-pressure vapor–liquid equilibria were investigated for binary protic ILs and CH<sub>4</sub></li> <li>The experimental data were collected by employing the static-synthetic visual strategy by a variable-volume cell unit, and results were verified by equilibrium data.</li> <li>ILs structure and purity were validated by FT-IR spectroscopy and <sup>1</sup>H and <sup>13</sup>C NMR investigations.</li> <li>Fischer volumetric was used to measure Water content.</li> <li>The three-parametric Redlich–Kwong–Peng–Robinson (RKPR) EoS model was developed to calculate the Henry’s law constants</li> </ul>	<ul style="list-style-type: none"> <li>N-methyl-2-hydroxyethylammonium propanoate [m-2HEA][Pr]</li> <li>Bis(2-hydroxyethyl) ammonium butanoate [BHEA][Bu]</li> </ul>	<ul style="list-style-type: none"> <li>Both ILs showed very low solubility for CH<sub>4</sub>, without temperature influence.</li> </ul>	[50]
<ul style="list-style-type: none"> <li>The GC-sPC-SAFT (Group Contribution Simplified Perturbed Chain Statistical Associating Fluid Theory) EoS was used to estimate CH<sub>4</sub> solubilities in ILs and correlate thermophysical properties of ILs.</li> </ul>	<ul style="list-style-type: none"> <li>[Cn-mim][BF<sub>4</sub>]</li> <li>[Cn-mim][PF<sub>6</sub>]</li> <li>[Cn-mim][NTf<sub>2</sub>]</li> </ul>	<ul style="list-style-type: none"> <li>The results favourably predicted the solubility of CH<sub>4</sub> with high accuracy</li> </ul>	[99]
<ul style="list-style-type: none"> <li>The constant of Henry’s law and thermodynamic characteristics, including enthalpy and entropy at an infinite dilution, were calculated from the experimental data of CH<sub>4</sub> solubility.</li> </ul>	<ul style="list-style-type: none"> <li>1-butylpyridinium bis(trifluoromethylsulfonyl)imide ([C<sub>4</sub>py][Tf<sub>2</sub>N])</li> <li>1-hexylpyridinium bis(trifluoromethylsulfonyl)imide ([C<sub>6</sub>py][Tf<sub>2</sub>N])</li> <li>1-butylpyridinium tetrafluoroborate ([C<sub>4</sub>py][BF<sub>4</sub>])</li> <li>1-hexylpyridinium tetrafluoroborate ([C<sub>6</sub>py][BF<sub>4</sub>])</li> </ul>	<ul style="list-style-type: none"> <li>The experimental results confirmed that CH<sub>4</sub> solubility increases with rising pressure and reducing temperature.</li> <li>The CH<sub>4</sub> solubility in ILs ranked: [C<sub>4</sub>py][BF<sub>4</sub>] &lt; [C<sub>6</sub>py][BF<sub>4</sub>] &lt; [C<sub>4</sub>py][Tf<sub>2</sub>N] &lt; [C<sub>6</sub>py][Tf<sub>2</sub>N].</li> </ul>	[100]
<ul style="list-style-type: none"> <li>The solubility of CH<sub>4</sub> in several ILs was determined experimentally at various temperatures (298.15 to 343.15 K) and pressures up to 8 MPa.</li> <li>The constants of Henry’s law values were measured by experimental solubility data of CH<sub>4</sub>.</li> <li>The effect of the cation and anion head group and the length of the alkyl chain on CH<sub>4</sub> solubility were investigated.</li> <li>A detailed investigation based on the Conductor-like Screening Model for Real Solvent (COSMO-RS) was performed to identify the molecular mechanism that governs CH<sub>4</sub> solubility in ILs.</li> </ul>	<ul style="list-style-type: none"> <li>[C<sub>4</sub>C<sub>1</sub>im][Ac]</li> <li>[C<sub>4</sub>C<sub>1</sub>im][BF<sub>4</sub>]</li> <li>[C<sub>4</sub>C<sub>1</sub>im][DMP]</li> <li>[C<sub>4</sub>C<sub>1</sub>im][DBP]</li> <li>[C<sub>4</sub>C<sub>1</sub>im][PF<sub>6</sub>]</li> <li>[C<sub>4</sub>C<sub>1</sub>im][SCN]</li> <li>[C<sub>4</sub>C<sub>1</sub>im][MeSO<sub>4</sub>]</li> <li>[C<sub>4</sub>C<sub>1</sub>im][OcSO<sub>4</sub>]</li> <li>[C<sub>4</sub>C<sub>1</sub>im][TFA]</li> <li>[C<sub>4</sub>C<sub>1</sub>im][Tf<sub>2</sub>N]</li> <li>[C<sub>4</sub>C<sub>1</sub>pip][Tf<sub>2</sub>N]</li> <li>[C<sub>4</sub>C<sub>1</sub>pyrr][Tf<sub>2</sub>N]</li> <li>[C<sub>4</sub>C<sub>1</sub>py][Tf<sub>2</sub>N]</li> <li>[C<sub>1</sub>C<sub>1</sub>im][Tf<sub>2</sub>N]</li> <li>[C<sub>2</sub>C<sub>1</sub>im][Tf<sub>2</sub>N]</li> <li>[C<sub>6</sub>C<sub>1</sub>im][Tf<sub>2</sub>N]</li> <li>[C<sub>10</sub>C<sub>1</sub>im][Tf<sub>2</sub>N]</li> </ul>	<ul style="list-style-type: none"> <li>The experimental results showed that CH<sub>4</sub> solubility in ILs enhances with a reducing temperature and increasing pressure.</li> <li>CH<sub>4</sub> solubility in ILs enhances with increasing the alkyl chain length of the cation or anion.</li> <li>The COSMO-RS model is an efficient and novel a priori predictive model for estimating the CH<sub>4</sub> solubility in ILs without access to experimental data.</li> </ul>	[101]

Table 13. Cont.

Highlights	ILs Used in the Study	Results	References
<ul style="list-style-type: none"> <li>Provides an overview of the recent developments and applications of Ionic Liquid Membranes (ILMs) for gas separation by focusing on the separation of carbon dioxide (CO<sub>2</sub>), methane (CH<sub>4</sub>), nitrogen (N<sub>2</sub>), hydrogen (H<sub>2</sub>), or mixtures of these gases from various gas streams.</li> </ul>	<ul style="list-style-type: none"> <li>The three general types of Ionic Liquid Membranes (ILMs), such as Supported Ionic Liquid Membranes (SILMs), Ionic Liquid Polymeric Membranes (ILPMs), and Ionic Liquid Mixed-Matrix Membranes (ILMMM)s</li> </ul>	<ul style="list-style-type: none"> <li>SILMs, ILPMs, and ILMMs are very promising membranes that have great potential in gas separation processes.</li> <li>They offer a wide range of permeabilities and selectivities for CO<sub>2</sub>, CH<sub>4</sub>, N<sub>2</sub>, H<sub>2</sub>, or mixtures of these gases.</li> </ul>	[102]
<ul style="list-style-type: none"> <li>The commercial software Multiflash and its interface with Excel were employed to calculate methane hydrate equilibrium conditions in the presence of imidazolium based ionic liquids.</li> </ul>	<ul style="list-style-type: none"> <li>[BMIM][BF<sub>4</sub>]</li> <li>[EMIM][BF<sub>4</sub>]</li> <li>[EMIM][Cl]</li> <li>[BMIM][Cl]</li> <li>[HMIM][Cl]</li> <li>[OMIM][Cl]</li> <li>[DMIM][Cl]</li> <li>[BMIM][Br]</li> <li>[BMIM][CH<sub>3</sub>SO<sub>4</sub>]</li> <li>[BMIM][HSO<sub>4</sub>]</li> <li>[BMIM][PF<sub>6</sub>]</li> <li>[BMIM][Ac]</li> <li>[BMIM][N(CN)<sub>2</sub>]</li> </ul>	<ul style="list-style-type: none"> <li>It was noticed that prediction accuracy decreases for the models as cation carbon chains increase, as non-ideality in water-IL is boosted by cation hydrophobicity.</li> </ul>	[103]

## 7. Conclusions

This study provides a critical examination of recent advancements and innovations for CH<sub>4</sub> capture by ILs. ILs have been considered as novel alternative solvents for CH<sub>4</sub> absorption due to their tremendous benefits, such as thermal stability, negligible vapor pressure, low heat capacity, and tuneable physicochemical properties. In addition to the advantages listed above, ILs also have a number of other properties that make them attractive for use in the after treatment of VAM. For example, ILs are non-flammable and non-toxic, which makes them safer to handle than conventional solvents. This approach contributes to reducing emissions of CH<sub>4</sub> from ventilation air, and CH<sub>4</sub> recovered from IL has a potential to be used as a source of energy.

The absorption of CH<sub>4</sub> in ionic liquids from the experimental and thermodynamic aspects was reviewed in this work. Based on what has been reviewed in this study, CH<sub>4</sub> has a much lower solubility in ILs compared to CO<sub>2</sub>, but it is higher than that of H<sub>2</sub>, CO, and N<sub>2</sub>. The literature has also proven that the presence of CO<sub>2</sub> increases the solubility of CH<sub>4</sub>. The experimental data of CH<sub>4</sub> solubility in ILs have confirmed that CH<sub>4</sub> solubility in ILs improves by increasing the pressure and reducing the temperature; therefore, low temperature is more suitable for enhancing CH<sub>4</sub> solubility in ILs. Furthermore, the IL with the highest solubility has the lowest Henry's law constant.

Regarding IL structures, increasing the alkyl chain length on the cation and anion significantly enhances the CH<sub>4</sub> solubility in ILs. In this regard, imidazolium-based ILs, with a long alkyl chain, demonstrated high solubility for CH<sub>4</sub>, mainly due to lower surface tension and molar density and the presence of large nonpolar alkyl-chains, which results in interaction with nonpolar CH<sub>4</sub> molecules. Moreover, it appeared that the [Tf<sub>2</sub>N] anion plays the most crucial role in the solubility of CH<sub>4</sub> because CH<sub>4</sub> solubility improves with fluoroalkyl groups present in the anion part. Finally, the data demonstrated that 1-butyl-3-methylimidazolium bis(trifluoromethylsulfonyl) imide [bmim][Tf<sub>2</sub>N] has a great potential and remarkable capacity to dissolve CH<sub>4</sub>.

Experimental limitations for the measurement of CH<sub>4</sub> solubility along with time-consuming experimental methods and costly operations are the major reasons for implementing artificial intelligence and thermodynamic procedures to describe the interactions and phase equilibrium of CH<sub>4</sub> in various ILs. Therefore, many efforts have been made by researchers to model or correlate the solubilities of CH<sub>4</sub> in ILs with thermodynamic

equations of state, such as the extended Henry's law model, the extended Pitzer's model, the Peng–Robinson equation of state, and the Krichevsky–Kasarnovsky equation, that have been reviewed in this study in depth. Nonetheless, the thermodynamic equations of state must be optimized based on experimental data, without which most of the proposed models cannot be reliable. On this point, the neural network method is a promising method that has been employed to model and predict CH<sub>4</sub> solubility and its phase equilibrium in different ILs. The COSMO-RS model is another novel a priori predictive model for estimating CH<sub>4</sub> absorption in ILs without relying on experimental data.

## 8. Medium and Long-Term Perspectives of VAM Abatement Using ILs

Reducing greenhouse gas emissions from Ventilation Air Methane (VAM) using ILs has promising long-term perspectives. VAM is a significant source of methane emissions from coal mines, and ionic liquids can effectively capture and convert this methane stream into usable fuel. This technology is sustainable, energy-efficient, and can significantly reduce the greenhouse gas emissions from coal mines. Furthermore, ILs are stable with significantly low vapor pressure values and, as such, can be reused multiple times, making them a cost-effective solution for VAM mitigation. However, further research and development are needed to optimize the performance of IL-based VAM capture systems and scale them up for commercial use. Another primary concern is the cost of IL synthesis for large-scale operations. Overall, the use of ionic liquids for VAM capture has significant potential to contribute to the reduction of greenhouse gas emissions and the transition towards a more sustainable energy future.

**Author Contributions:** Conceptualization, J.Z. and B.M.; methodology, H.R.R., validation, H.R.R. and J.Z.; formal analysis, H.R.R.; investigation, H.R.R.; resources, J.Z.; data curation, H.R.R.; writing—original draft preparation, H.R.R.; writing—review and editing, J.Z.; visualization, H.R.R.; supervision, J.Z., B.M.; project administration, J.Z.; funding acquisition, B.M. All authors have read and agreed to the published version of the manuscript.

**Funding:** This research received no external funding.

**Institutional Review Board Statement:** Not applicable.

**Informed Consent Statement:** Not applicable.

**Data Availability Statement:** The data presented in this study are openly available in a publicly accessible repository.

**Conflicts of Interest:** The authors declare no conflict of interest.

## Appendix A

**Table A1.** Critical properties of imidazolium-based ionic liquids (including 30 different types of anions) estimated using the modified Lydersen–Joback–Reid method [79,80].

No.	IL	IUPAC Name	$M$ ( $\text{gmol}^{-1}$ )	$\omega$	$T_C$ (K)	$P_C$ (bar)	$T_b$ (K)
1	[emim] [tsac]	1-ethyl-3-methylimidazolium [2,2,2-trifluoro-n- (trifluoromethyl)sulfonyl]acetamide	355.3	0.4981	1069.9	25.2	764.4
2.1	[bmim] [TFES]	1-butyl-3-methylimidazolium 1,1,2,2-tetrafluoroethanesulfonate	320.3	0.4583	1030.5	25.7	729.4
2.2	[C <sub>12</sub> mim] [TFES]	1-dodecyl-3-methylimidazolium 1,1,2,2-tetrafluoroethanesulfonate	432.5	0.8065	1171.0	15.6	912.5
2.3	[emim] [TFES]	1-ethyl-3-methylimidazolium 1,1,2,2-tetrafluoroethanesulfonate	292.3	0.3743	998.2	30.4	683.7
2.4	[hpmim] [TFES]	1-heptyl-3-methylimidazolium 1,1,2,2-tetrafluoroethanesulfonate	362.4	0.5903	1080.8	20.7	798.1

Table A1. Cont.

No.	IL	IUPAC Name	$M$ ( $\text{gmol}^{-1}$ )	$\omega$	$T_C$ (K)	$P_C$ (bar)	$T_b$ (K)
3	[bmim] [HFPS]	1-butyl-3-methylimidazolium 1,1,2,3,3,3-hexafluoropropanesulfonate	370.3	0.4933	1032.1	21.3	747.6
4	[bmim] [TPES]	1-butyl-3-methylimidazolium 1,1,2-trifluoro- 2-(perfluoroethoxy)ethanesulfonate	436.3	0.5488	1061.3	17.9	788.2
5	[bmim] [TTES]	1-butyl-3-methylimidazolium 1,1,2- trifluoro-2- (trifluoromethoxy)ethanesulfonate	386.3	0.5085	1058.3	20.9	770.0
6	[bmim] [FS]	1-butyl-3-methylimidazolium 2-(1,2,2,2-tetrafluoroethoxy)-1,1,2,2- tetrafluoroethanesulfonate	436.3	0.5488	1061.3	17.9	788.2
7.1	[bmim] [Ac]	1-butyl-3-methylimidazolium acetate	198.3	0.6681	847.3	24.5	624.6
7.2	[emim] [Ac]	1-ethyl-3-methylimidazolium acetate	170.2	0.5889	807.1	29.2	578.8
8.1	[emim] [BEI]	1-ethyl-3-methylimidazolium bis(pentafluoroethylsulfonyl)imide	491.3	0.2895	1231.4	21.9	853.1
8.2	[bmim] [BEI]	1-butyl-3-methylimidazolium bis(pentafluoroethylsulfonyl)imide	519.4	0.3812	1257.1	19.5	898.8
9.1	[beim] [Tf <sub>2</sub> N]	1-butyl-3-ethylimidazolium bis[(trifluoromethyl)sulfonyl]imide	433.4	0.3444	1281.1	25.6	885.3
9.2	[bmim] [Tf <sub>2</sub> N]	1-butyl-3-methylimidazolium bis[(trifluoromethyl)sulfonyl]imide	419.4	0.3004	1269.9	27.6	862.4
9.3	[deim] [Tf <sub>2</sub> N]	1,3-diethylimidazolium bis[(trifluoromethyl)sulfonyl]imide	405.3	0.2575	1259.3	30.0	839.6
9.4	[edmim] [Tf <sub>2</sub> N]	1-ethyl-2,3-dimethylimidazolium bis[(trifluoromethyl)sulfonyl]imide	405.3	0.2794	1258.9	29.8	844.5
9.5	[eDmim] [Tf <sub>2</sub> N]	1-ethyl-3,5-dimethylimidazolium bis[(trifluoromethyl)sulfonyl]imide	405.3	0.2794	1258.9	29.8	844.5
9.6	[emim] [Tf <sub>2</sub> N]	1-ethyl-3-methylimidazolium bis[(trifluoromethyl)sulfonyl]imide	391.3	0.2157	1249.3	32.7	816.7
9.7	[hmim] [Tf <sub>2</sub> N]	1-hexyl-3-methylimidazolium bis[(trifluoromethyl)sulfonyl]imide	447.4	0.3893	1292.8	23.9	908.2
9.8	[ibmim] [Tf <sub>2</sub> N]	1-isobutyl-3-methylimidazolium bis[(trifluoromethyl)sulfonyl]imide	419.4	0.2846	1275.2	27.9	862.0
9.9	[mdeim] [Tf <sub>2</sub> N]	5-methyl-1,3-diethylimidazolium bis[(trifluoromethyl)sulfonyl]imide	419.4	0.3226	1269.7	27.5	867.4
9.10	[meim] [Tf <sub>2</sub> N]	1-methyl-3-ethylimidazolium bis[(trifluoromethyl)sulfonyl]imide	391.3	0.2157	1249.3	32.7	816.7
9.11	[moemim] [Tf <sub>2</sub> N]	1-methoxyethyl-3-methylimidazolium bis[(trifluoromethyl)sulfonyl]imide	421.3	0.2695	1285.2	29.1	862.0
9.12	[omim] [Tf <sub>2</sub> N]	1-octyl-3-methylimidazolium bis[(trifluoromethyl)sulfonyl]imide	475.5	0.4811	1317.8	21.0	954.0
9.13	[prdmim] [Tf <sub>2</sub> N]	1-propyl-2,3-dimethylimidazolium bis[(trifluoromethyl)sulfonyl]imide	419.4	0.3226	1269.7	27.5	867.4
9.14	[C <sub>3</sub> (mim) <sub>2</sub> ] [Tf <sub>2</sub> N] <sub>2</sub>	1,3-di(3-methylimidazolium)propane di-bis[(trifluoromethyl)sulfonyl]imide	766.6	0.2458	2033.6	19.5	1410.9
9.15	[C <sub>6</sub> (mim) <sub>2</sub> ] [Tf <sub>2</sub> N] <sub>2</sub>	1,6-di(3-methylimidazolium)hexane di-bis[(trifluoromethyl)sulfonyl]imide	808.7	0.3899	2037.2	16.9	1479.5
9.16	[C <sub>9</sub> (mim) <sub>2</sub> ] [Tf <sub>2</sub> N] <sub>2</sub>	1,9-di(3-methylimidazolium)nonane di-bis[(trifluoromethyl)sulfonyl]imide	850.8	0.5354	2052.8	14.8	1548.2

Table A1. Cont.

No.	IL	IUPAC Name	$M$ ( $\text{gmol}^{-1}$ )	$\omega$	$T_C$ (K)	$P_C$ (bar)	$T_b$ (K)
9.17	[C <sub>12</sub> (mim) <sub>2</sub> ][Tf <sub>2</sub> N] <sub>2</sub>	1,12-di(3-methylimidazolium)dodecane di-bis[(trifluoromethyl)sulfonyl]imide	892.8	0.6748	2079.4	13.2	1616.8
9.18	[C <sub>9</sub> (bim) <sub>2</sub> ][Tf <sub>2</sub> N] <sub>2</sub>	1,9-di(3-butylimidazolium)nonane di-bis[(trifluoromethyl)sulfonyl]imide	934.9	0.7974	2079.4	11.9	1685.4
9.19	[C <sub>9</sub> (m <sub>2</sub> mim) <sub>2</sub> ][Tf <sub>2</sub> N] <sub>2</sub>	1,9-di(2,3-dimethylimidazolium)nonane di-bis[(trifluoromethyl)sulfonyl]imide	878.8	0.7974	2069.1	13.6	1603.9
9.20	[C <sub>12</sub> (benzimid) <sub>2</sub> ][Tf <sub>2</sub> N] <sub>2</sub>	1,12-di(3-benzylimidazolium)dodecane di-bis[(trifluoromethyl)sulfonyl]imide	1045.0	0.8928	2395.1	10.6	1944.7
9.21	[dmprim][Tf <sub>2</sub> N]	1,2-dimethyl-3-propylimidazolium bis[(trifluoromethyl)sulfonyl]imide	419.4	0.3226	1269.7	27.5	867.4
9.22	[dbim][Tf <sub>2</sub> N]	1,3-dibutylimidazolium bis[(trifluoromethyl)sulfonyl]imide	461.5	0.4349	1305.0	22.3	931.1
9.23	[E1,3M4I][Tf <sub>2</sub> N]	1,3-diethyl-4-methylimidazolium bis[(trifluoromethyl)sulfonyl]imide	419.4	0.3226	1269.7	27.5	867.4
9.24	[dmim][Tf <sub>2</sub> N]	1,3-dimethylimidazolium bis[(trifluoromethyl)sulfonyl]imide	377.3	0.1752	1239.9	35.8	793.8
9.25	[C10mim][Tf <sub>2</sub> N]	1-decyl-3-methylimidazolium bis[(trifluoromethyl)sulfonyl]imide	503.5	0.5741	1345.1	18.7	999.7
9.26	[hpmim][Tf <sub>2</sub> N]	1-heptyl-3-methylimidazolium bis[(trifluoromethyl)sulfonyl]imide	461.5	0.4349	1305.0	22.3	931.1
9.27	[nmim][Tf <sub>2</sub> N]	1-nonyl-3-methylimidazolium bis[(trifluoromethyl)sulfonyl]imide	489.5	0.5276	1331.2	19.8	976.8
9.28	[pmim][Tf <sub>2</sub> N]	1-pentyl-3-methylimidazolium bis[(trifluoromethyl)sulfonyl]imide	433.4	0.3444	1281.1	25.6	885.3
9.29	[prmim][Tf <sub>2</sub> N]	1-propyl-3-methylimidazolium bis[(trifluoromethyl)sulfonyl]imide	405.3	0.2575	1259.3	30.0	839.6
9.30	[dmeim][Tf <sub>2</sub> N]	1,2-dimethyl-3-ethylimidazolium bis[(trifluoromethyl)sulfonyl]imide	405.3	0.2794	1258.9	29.8	844.5
9.31	[eomim][Tf <sub>2</sub> N]	ethoxymethyl-3-methylimidazolium bis[(trifluoromethyl)sulfonyl]imide	421.3	0.2695	1285.2	29.1	862.0
9.32	[Ph(CH <sub>2</sub> )mim][Tf <sub>2</sub> N]	1-(1-phenylalkyl)-3-methylimidazolium bis[(trifluoromethyl)sulfonyl]imide	453.4	0.3037	1405.9	27.0	957.8
9.33	[Ph(CH <sub>2</sub> ) <sub>2</sub> mim][Tf <sub>2</sub> N]	1-(2-phenylalkyl)-3-methylimidazolium bis[(trifluoromethyl)sulfonyl]imide	467.4	0.3484	1414.8	25.1	980.6
9.34	[Ph(CH <sub>2</sub> ) <sub>3</sub> mim][Tf <sub>2</sub> N]	1-(3-phenylalkyl)-3-methylimidazolium bis[(trifluoromethyl)sulfonyl]imide	481.4	0.3939	1424.5	23.4	1003.5
9.35	[bdmim][Tf <sub>2</sub> N]	1-butyl-2,3-dimethylimidazolium bis[(trifluoromethyl)sulfonyl]imide	433.4	0.3669	1281.1	25.5	890.3
9.36	[C <sub>12</sub> mim][Tf <sub>2</sub> N]	1-dodecyl-3-methylimidazolium bis[(trifluoromethyl)sulfonyl]imide	531.6	0.6662	1374.6	16.8	1045.5
9.37	[memim][Tf <sub>2</sub> N]	1-methyl-3-ethyl-4-methylimidazolium bis[(trifluoromethyl)sulfonyl]imide	405.3	0.2794	1258.9	29.8	844.5
9.38	[hdmim][Tf <sub>2</sub> N]	1-hexyl-2,3-dimethylimidazolium bis[(trifluoromethyl)sulfonyl]imide	461.5	0.4578	1305.5	22.2	936.1
9.39	[C <sub>2</sub> F <sub>3</sub> mim][Tf <sub>2</sub> N]	1-trifluoroethyl-3-methylimidazolium bis[(trifluoromethyl)sulfonyl]imide	445.3	0.2338	1210.5	26.7	811.3
10.1	[bmim][Br]	1-butyl-3-methylimidazolium bromide	219.1	0.4891	834.9	29.8	586.8
10.2	[pmim][Br]	1-pentyl-3-methylimidazolium bromide	233.2	0.5292	854.2	27.2	609.6

Table A1. Cont.

No.	IL	IUPAC Name	$M$ ( $\text{gmol}^{-1}$ )	$\omega$	$T_C$ (K)	$P_C$ (bar)	$T_b$ (K)
10.3	[C <sub>9</sub> (mim) <sub>2</sub> ][Br]	1,9-di(3-methylimidazolium)nonane dibromide	450.3	0.9068	1270.4	16.6	996.8
10.4	[C <sub>12</sub> (mim) <sub>2</sub> ][Br]	1,12-di(3-methylimidazolium)dodecane dibromide	492.3	1.0089	1328.7	14.4	1065.4
10.5	[C <sub>9</sub> (bim) <sub>2</sub> ][Br]	1,9-di(3-butylimidazolium)nonane dibromide	534.4	1.0752	1392.3	12.6	1134.1
11.1	[bmim][Cl]	1-butyl-3-methylimidazolium chloride	174.7	0.4914	789.0	27.8	558.0
11.2	[hmim][Cl]	1-hexyl-3-methylimidazolium chloride	202.7	0.5725	829.2	23.5	603.8
11.3	[omim][Cl]	1-octyl-3-methylimidazolium chloride	230.8	0.6566	869.4	20.3	649.6
11.4	[Bemim][Cl]	1-benzyl-3-methylimidazolium chloride	208.7	0.5145	921.3	28.4	653.4
11.5	[C <sub>12</sub> mim][Cl]	1-dodecyl-3-methylimidazolium chloride	286.9	0.8212	951.5	16.0	741.1
11.6	[emim][Cl]	1-ethyl-3-methylimidazolium chloride	146.6	0.4165	748.6	34.2	512.3
11.7	[mmim][Cl]	1-methyl-3-methylimidazolium chloride	132.6	0.3825	728.2	38.5	489.4
11.8	[mim][Cl]	1-methylimidazolium chloride	118.6	0.4158	677.8	48.1	450.5
11.9	[C <sub>1</sub> Benmim][Cl]	1-p-chlorobenzyl-3-methylimidazolium chloride	243.1	0.5521	969.6	26.8	695.8
11.10	[FBenmim][Cl]	1-p-fluorobenzyl-3-methylimidazolium chloride	226.7	0.5660	913.1	26.4	657.6
11.11	[dbim][Cl]	1,3-dibutylimidazolium chloride	216.8	0.6144	849.2	21.8	626.7
11.12	[C <sub>5</sub> O <sub>2</sub> mim][Cl]	1-[2-(methoxyethoxy)-ethyl]-3-methylimidazolium chloride	220.7	0.5707	863.6	24.8	625.8
11.13	[moim][Cl]	1-methyl-3-octylimidazolium chloride	230.8	0.6566	869.4	20.3	649.6
12.1	[bmim][DCA]	1-butyl-3-methylimidazolium dicyanamide	205.3	0.8419	1035.8	24.4	783.0
12.2	[emim][DCA]	1-ethyl-3-methylimidazolium dicyanamide	177.2	0.7661	999.0	29.1	737.2
12.3	[omim][DCA]	1-octyl-3-methylimidazolium dicyanamide	261.4	0.9908	1113.1	18.4	874.5
13	[emim][DEGlyMSO <sub>4</sub> ]	1-ethyl-3-methylimidazolium diethyleneglycol monomethylethersulfate	310.4	0.5176	1162.9	28.1	826.2
14	[dmim][DMPO <sub>4</sub> ]	1,3-dimethylimidazolium dimethylphosphate	222.2	0.5973	816.8	27.2	590.0
15.1	[edmim][EtSO <sub>4</sub> ]	1-ethyl-2,3-dimethylimidazolium ethylsulfate	250.3	0.4341	1082.6	35.8	740.5
15.2	[emim][EtSO <sub>4</sub> ]	1-ethyl-3-methylimidazolium ethylsulfate	236.3	0.3744	1067.5	40.5	712.7
16.1	[omim][PF <sub>6</sub> ]	1-octyl-3-methylimidazolium hexafluorophosphate	340.3	0.9385	810.8	14.0	646.1
16.2	[bmim][PF <sub>6</sub> ]	1-butyl-3-methylimidazolium hexafluorophosphate	284.2	0.7917	719.4	17.3	554.6
16.3	[emim][PF <sub>6</sub> ]	1-ethyl-3-methylimidazolium hexafluorophosphate	256.1	0.7083	674.0	19.5	508.8
16.4	[hmim][PF <sub>6</sub> ]	1-hexyl-3-methylimidazolium hexafluorophosphate	312.2	0.8697	764.9	15.5	600.3

Table A1. Cont.

No.	IL	IUPAC Name	$M$ ( $\text{gmol}^{-1}$ )	$\omega$	$T_C$ (K)	$P_C$ (bar)	$T_b$ (K)
16.5	[bdmim] [PF <sub>6</sub> ]	1-butyl-2,3-dimethylimidazolium hexafluorophosphate	298.2	0.8526	746.3	16.2	582.4
16.6	[hpmim] [PF <sub>6</sub> ]	1-heptyl-3-methylimidazolium hexafluorophosphate	326.3	0.9055	787.8	14.7	623.2
16.7	[nmim] [PF <sub>6</sub> ]	1-nonyl-3-methylimidazolium hexafluorophosphate	354.3	0.9680	834.1	13.4	669.0
16.8	[oprim] [PF <sub>6</sub> ]	1-octyl-3-propylimidazolium hexafluorophosphate	368.3	0.9937	857.6	12.8	691.9
16.9	[pmim] [PF <sub>6</sub> ]	1-pentyl-3-methylimidazolium hexafluorophosphate	298.2	0.8316	742.1	16.3	577.5
16.10	[eommim] [PF <sub>6</sub> ]	ethoxymethyl-3-methylimidazolium hexafluorophosphate	286.2	0.8316	723.7	18.2	554.1
16.11	[mommim] [PF <sub>6</sub> ]	methyloxymethyl-3-methylimidazolium hexafluorophosphate	272.1	0.7277	701.2	19.3	531.2
16.12	[Ph(CH <sub>2</sub> ) <sub>3</sub> mim] [PF <sub>6</sub> ]	1-(3-phenylalkyl)-3-methylimidazolium hexafluorophosphate	346.3	0.8894	885.1	15.7	695.7
16.13	[prmim] [PF <sub>6</sub> ]	1-propyl-3-methylimidazolium hexafluorophosphate	270.2	0.7504	696.7	18.3	531.7
16.14	[hemim][PF <sub>6</sub> ]	1-hexyl-3-ethylimidazolium hexafluorophosphate	326.3	0.9055	787.8	14.7	623.2
16.15	[odmim] [PF <sub>6</sub> ]	1-octyl-2,3-dimethylimidazolium hexafluorophosphate	354.3	0.9680	834.1	13.4	669.0
16.16	[C <sub>2</sub> OHmim] [PF <sub>6</sub> ]	1-(2-hydroxyethyl)-3-methylimidazolium hexafluorophosphate	272.1	1.0367	766.9	20.2	601.0
16.17	[C <sub>3</sub> Omim] [PF <sub>6</sub> ]	1-propoxymethyl-3-methylimidazolium hexafluorophosphate	286.2	0.7697	723.7	18.2	554.1
16.18	[C <sub>5</sub> O <sub>2</sub> mim] [PF <sub>6</sub> ]	1-[2-(methoxyethoxy)-ethyl]-3-methylimidazolium hexafluorophosphate	330.2	0.8676	795.3	16.1	622.3
16.19	[C <sub>12</sub> (mim) <sub>2</sub> ] [PF <sub>6</sub> ]	1-[2-(methoxyethoxy)-ethyl]-3-methylimidazolium hexafluorophosphate	622.5	0.8285	1219.8	8.5	1001.1
16.20	[C <sub>9</sub> (bim) <sub>2</sub> ] [PF <sub>6</sub> ]	1,9-di(3-butylimidazolium)nonane bis(hexafluorophosphate)	664.5	0.6496	1318.6	7.9	1069.7
16.21	[C <sub>12</sub> (benzim) <sub>2</sub> ] [PF <sub>6</sub> ]	1,12-di(3-benzylimidazolium)dodecane bis(hexafluorophosphate)	774.7	0.4407	1671.1	7.4	1329.0
16.22	[moim] [PF <sub>6</sub> ]	1-methyl-3-octylimidazolium hexafluorophosphate	340.3	0.9385	810.8	14.0	646.1
17.1	[bdmim] [BF <sub>4</sub> ]	1-butyl-2,3-dimethylimidazolium tetrafluoroborate	240.1	0.9476	523.1	18.9	523.1
17.2	[C <sub>10</sub> mim] [BF <sub>4</sub> ]	1-decyl-3-methylimidazolium tetrafluoroborate	310.2	1.0818	632.5	14.5	632.5
17.3	[moemim] [BF <sub>4</sub> ]	ethyloxymethyl-3-methylimidazolium tetrafluoroborate	228.0	0.8692	494.8	21.7	494.8
17.4	[prmim] [BF <sub>4</sub> ]	1-propyl-3-methylimidazolium tetrafluoroborate	212.0	0.8485	472.3	21.9	472.3
17.5	[mommim] [BF <sub>4</sub> ]	methyloxymethyl-3-methylimidazolium tetrafluoroborate	214.0	0.8296	471.9	23.3	471.9

Table A1. Cont.

No.	IL	IUPAC Name	$M$ ( $\text{gmol}^{-1}$ )	$\omega$	$T_C$ (K)	$P_C$ (bar)	$T_b$ (K)
17.6	[DEME] [BF <sub>4</sub> ]	N,N-diethyl-N-methyl-N-(2-methoxyethyl)ammonium tetrafluoroborate	233.1	0.9465	393.5	17.1	393.5
17.7	[bmim] [BF <sub>4</sub> ]	1-butyl-3-methylimidazolium tetrafluoroborate	226.0	0.8877	495.2	20.4	495.2
17.8	[emim] [BF <sub>4</sub> ]	1-ethyl-3-methylimidazolium tetrafluoroborate	198.0	0.8087	449.5	23.6	449.5
17.9	[hmim] [BF <sub>4</sub> ]	1-hexyl-3-methylimidazolium tetrafluoroborate	254.1	0.9625	690.0	17.9	541.0
17.10	[omim] [BF <sub>4</sub> ]	1-octyl-3-methylimidazolium tetrafluoroborate	282.1	1.0287	737.0	16.0	586.7
17.11	[moim] [BF <sub>4</sub> ]	1-methyl-3-octylimidazolium tetrafluoroborate	282.1	1.0287	737.0	16.0	586.7
17.12	[C <sub>2</sub> OHmim] [BF <sub>4</sub> ]	1-(2-hidroxyethyl)-3-methylimidazolium tetrafluoroborate	214.0	1.1643	691.9	24.7	541.6
17.13	[C <sub>3</sub> Oim] [BF <sub>4</sub> ]	1-propoxymethyl-3-methylimidazolium tetrafluoroborate	228.0	0.8692	647.0	21.7	494.8
17.14	[C <sub>5</sub> O <sub>2</sub> mim] [BF <sub>4</sub> ]	1-[2-(methoxyethoxy)-ethyl]-3-methylimidazolium tetrafluoroborate	272.1	0.9644	720.2	18.8	562.9
17.15	[C <sub>12</sub> (mim) <sub>2</sub> ] [BF <sub>4</sub> ]	1,12-di(3-methylimidazolium)dodecane bis(tetrafluoroborate)	506.1	0.9804	1074.4	10.1	882.4
17.16	[C <sub>9</sub> (bim) <sub>2</sub> ] [BF <sub>4</sub> ]	1,9-di(3-butylimidazolium)nonane bis(tetrafluoroborate)	548.2	0.7841	1170.9	9.1	951.0
18.1	[bmim] [HSO <sub>4</sub> ]	1-propyl-3-methylimidazolium hexafluorophosphate	236.3	0.7034	1103.8	43.4	782.4
18.2	[emim] [HSO <sub>4</sub> ]	1-ethyl-3-methylimidazolium hydrogensulfate	208.2	0.6411	1073.8	57.6	736.7
18.3	[mim] [HSO <sub>4</sub> ]	1-methylimidazolium hydrogensulfate	180.2	0.6707	1012.7	91.9	674.9
19	[bmim] [I]	1-butyl-3-methylimidazolium iodide	266.1	0.4835	871.2	28.6	613.7
20.1	[bmim] [mesy]	1-butyl-3-methylimidazolium methanesulfonate	234.3	0.3990	1054.8	37.4	713.1
20.2	[emim] [mesy]	1-ethyl-3-methylimidazolium methanesulfonate	206.3	0.3307	1026.0	48.1	667.4
21	[dmim] [MOESO <sub>4</sub> ]	1,3-dimethylimidazolium methoxyethylsulfate	252.3	0.3855	1094.4	38.9	735.1
22.1	[dmim] [MeSO <sub>4</sub> ]	1,3-dimethylimidazolium methylsulfate	208.2	0.3086	1040.0	52.9	666.9
22.2	[bmim] [MeSO <sub>4</sub> ]	1-butyl-3-methylimidazolium methylsulfate	250.3	0.4111	1081.6	36.1	735.6
23	[bmim] [C <sub>8</sub> S]	1-butyl-3-methylimidazolium octylsulfate	348.5	0.7042	1189.8	20.2	895.7
24	[bmim] [tca]	1-butyl-3-methylimidazolium thiocyanate	197.3	0.4781	1047.4	19.4	763.1
25	[emim] [SCN]	1-ethyl-3-methylimidazolium thiocyanate	169.3	0.3931	1013.6	22.3	717.3
26	[bmim] [TMEM]	1-butyl-3-methylimidazolium tris(trifluoromethylsulfonyl)methide	550.4	0.1322	1571.4	24.0	1034.4

Table A1. Cont.

No.	IL	IUPAC Name	$M$ ( $\text{gmol}^{-1}$ )	$\omega$	$T_C$ (K)	$P_C$ (bar)	$T_b$ (K)
27.1	[emim] [ta]	1-ethyl-3-methylimidazolium trifluoroacetate	224.2	0.6051	785.3	24.3	573.4
27.2	[beim] [ta]	1-butyl-3-ethylimidazolium trifluoroacetate	266.3	0.7312	847.6	19.6	642.0
27.3	[bmim] [ta]	1-butyl-3-methylimidazolium trifluoroacetate	252.2	0.6891	826.8	20.9	619.2
27.4	[deim] [ta]	diethylimidazolium trifluoroacetate	238.2	0.6469	806.1	22.5	596.3
28	[bmim] [NO <sub>3</sub> ]	1-butyl-3-methylimidazolium nitrate	201.2	0.6436	954.8	27.3	694.9
29.1	[bmim] [NfO]	1-butyl-3-methylimidazolium nonafluorobutanesulfonate	438.3	0.5150	1028.8	17.3	762.3
29.2	[omim] [NfO]	1-octyl-3-methylimidazolium nonafluorobutanesulfonate	494.4	0.6926	1103.0	14.2	853.8
29.3	[beim] [NfO]	1-butyl-3-ethylimidazolium nonafluorobutanesulfonate	452.3	0.5605	1046.9	16.4	785.2
29.4	[emim] [NfO]	1-ethyl-3-methylimidazolium nonafluorobutanesulfonate	410.3	0.5605	993.4	19.4	716.5
30.1	[mopmi] [TfO]	1-(4-methoxyphenyl)-3-methylimidazolium trifluoromethanesulfonate	338.3	0.4481	1184.7	28.0	830.4
30.2	[dbim] [TfO]	1,3-dibutylimidazolium trifluoromethanesulfonate	330.4	0.5325	1072.0	23.2	776.4
30.3	[Bemim] [TfO]	1-benzyl-3-methylimidazolium trifluoromethanesulfonate	322.3	0.4118	1158.0	29.0	803.0
30.4	[omim] [TfO]	1-octyl-3-methylimidazolium trifluoromethanesulfonate	344.4	0.5766	1088.7	21.6	799.2
30.5	[beim] [TfO]	1-butyl-3-ethylimidazolium trifluoromethanesulfonate	302.3	0.4463	1039.5	27.0	730.6
30.6	[bmim] [TfO]	1-butyl-3-methylimidazolium trifluoromethanesulfonate	288.3	0.4046	1023.5	29.5	707.7
30.7	[deim] [TfO]	1,3-diethylimidazolium trifluoromethanesulfonate	274.3	0.3643	1007.8	32.4	684.8
30.8	[C <sub>12</sub> eim] [TfO]	1-dodecyl-3-ethylimidazolium trifluoromethanesulfonate	414.5	0.7935	1177.2	16.1	913.6
30.	[edmim] [TfO]	1-ethyl-3,5-dimethylimidazolium trifluoromethanesulfonate	274.3	0.3869	1177.2	32.1	689.8
30.	[emim] [TfO]	1-ethyl-3-methylimidazolium trifluoromethanesulfonate	260.2	0.3255	992.3	35.8	662.0

## References

- Wang, W.; Ren, J.; Li, X.; Li, H.; Li, D.; Li, H.; Song, Y. Enrichment experiment of ventilation air methane (0.5%) by the mechanical tower. *Sci. Rep.* **2020**, *10*, 7276. [[CrossRef](#)] [[PubMed](#)]
- Whiting, G.J.; Chanton, J.P. Greenhouse carbon balance of wetlands: Methane emission versus carbon sequestration. *Tellus B* **2001**, *53*, 521–528. [[CrossRef](#)]
- Karakurt, I.; Aydin, G.; Aydiner, K. Mine ventilation air methane as a sustainable energy source. *Renew. Sustain. Energy Rev.* **2011**, *15*, 1042–1049. [[CrossRef](#)]
- Kim, J.; Maiti, A.; Lin, L.-C.; Stolaroff, J.K.; Smit, B.; Aines, R.D. New materials for methane capture from dilute and medium-concentration sources. *Nat. Commun.* **2013**, *4*, 1694. [[CrossRef](#)] [[PubMed](#)]
- Somers, J.; Schultz, H. Thermal oxidation of coal mine ventilation air methane. In Proceedings of the 12th US/North American Mine Ventilation Symposium, Sparks, NV, USA, 9–11 June 2008.
- Somers, J. *Ventilation Air Methane (VAM) Utilization Technologies*; US EPA Coalbed Methane Outreach Program, Technical Options Series; United States Environmental Protection Agency: Washington, DC, USA, 2009.
- Setiawan, A.; Kennedy, E.M.; Stockenhuber, M. Development of Combustion Technology for Methane Emitted from Coal-Mine Ventilation Air Systems. *Energy Technol.* **2017**, *5*, 521–538. [[CrossRef](#)]

8. Su, S.; Chen, H.; Teakle, P.; Xue, S. Characteristics of coal mine ventilation air flows. *J. Environ. Manag.* **2008**, *86*, 44–62. [[CrossRef](#)] [[PubMed](#)]
9. Monai, M.; Montini, T.; Gorte, R.J.; Fornasiero, P. Catalytic oxidation of methane: Pd and beyond. *Eur. J. Inorg. Chem.* **2018**, *2018*, 2884–2893. [[CrossRef](#)]
10. Epling, W.S.; Hoflund, G.B. Catalytic oxidation of methane over ZrO<sub>2</sub>-supported Pd catalysts. *J. Catal.* **1999**, *182*, 5–12. [[CrossRef](#)]
11. Jiang, H.; Chen, Y.; Jiang, P.; Zhang, C.; Smith, T.J.; Murrell, J.C.; Xing, X.-H. Methanotrophs: Multifunctional bacteria with promising applications in environmental bioengineering. *Biochem. Eng. J.* **2010**, *49*, 277–288. [[CrossRef](#)]
12. Du, J.; Li, H.; Wang, L. Phase equilibria and methane enrichment of clathrate hydrates of mine ventilation air+ tetrabutylphosphonium bromide. *Ind. Eng. Chem. Res.* **2014**, *53*, 8182–8187. [[CrossRef](#)]
13. Gambelli, A.M.; Stornelli, G.; Di Schino, A.; Rossi, F. Methane and carbon dioxide hydrates properties in presence of Inconel 718 particles: Analyses on its potential application in gas separation processes to perform efficiency improvement. *J. Environ. Chem. Eng.* **2021**, *9*, 106571. [[CrossRef](#)]
14. Liu, G.; Zhu, L.; Cao, W.; Liu, H.; He, Y. New technique integrating hydrate-based gas separation and chemical absorption for the sweetening of natural gas with high H<sub>2</sub>S and CO<sub>2</sub> contents. *ACS Omega* **2021**, *6*, 26180–26190. [[CrossRef](#)]
15. Kamata, Y.; Oyama, H.; Shimada, W.; Ebinuma, T.; Takeya, S.; Uchida, T.; Nagao, J.; Narita, H. Gas separation method using tetra-n-butyl ammonium bromide semi-clathrate hydrate. *Jpn. J. Appl. Phys.* **2004**, *43*, 362. [[CrossRef](#)]
16. Carvalho, P.J.; Coutinho, J.A. The polarity effect upon the methane solubility in ionic liquids: A contribution for the design of ionic liquids for enhanced CO<sub>2</sub>/CH<sub>4</sub> and H<sub>2</sub>S/CH<sub>4</sub> selectivities. *Energy Environ. Sci.* **2011**, *4*, 4614–4619. [[CrossRef](#)]
17. Hojniak, S.D.; Khan, A.L.; Holloczki, O.; Kirchner, B.; Vankelecom, I.F.; Dehaen, W.; Binnemans, K. Separation of carbon dioxide from nitrogen or methane by supported ionic liquid membranes (SILMs): Influence of the cation charge of the ionic liquid. *J. Phys. Chem. B* **2013**, *117*, 15131–15140. [[CrossRef](#)]
18. Alonso, A.; Moral-Vico, J.; Markeb, A.A.; Busquets-Fité, M.; Komilis, D.; Puentes, V.; Sánchez, A.; Font, X. Critical review of existing nanomaterial adsorbents to capture carbon dioxide and methane. *Sci. Total Environ.* **2017**, *595*, 51–62. [[CrossRef](#)] [[PubMed](#)]
19. Li, D.; Chen, L.; Liu, G.; Yuan, Z.-Y.; Li, B.-F.; Zhang, X.; Wei, J.-Q. Porous metal–organic frameworks for methane storage and capture: Status and challenges. *New Carbon Mater.* **2021**, *36*, 468–496. (In Chinese) [[CrossRef](#)]
20. Makal, T.A.; Li, J.-R.; Lu, W.; Zhou, H.-C. Methane storage in advanced porous materials. *Chem. Soc. Rev.* **2012**, *41*, 7761–7779. [[CrossRef](#)] [[PubMed](#)]
21. Ramdin, M.; Amplianitis, A.; Bazhenov, S.; Volkov, A.; Volkov, V.; Vlugt, T.J.; de Loos, T.W. Solubility of CO<sub>2</sub> and CH<sub>4</sub> in ionic liquids: Ideal CO<sub>2</sub>/CH<sub>4</sub> selectivity. *Ind. Eng. Chem. Res.* **2014**, *53*, 15427–15435. [[CrossRef](#)]
22. Ramdin, M.; Chen, Q.; Balaji, S.P.; Vicent-Luna, J.M.; Torres-Knoop, A.; Dubbeldam, D.; Calero, S.; de Loos, T.W.; Vlugt, T.J. Solubilities of CO<sub>2</sub>, CH<sub>4</sub>, C<sub>2</sub>H<sub>6</sub>, and SO<sub>2</sub> in ionic liquids and Selexol from Monte Carlo simulations. *J. Comput. Sci.* **2016**, *15*, 74–80. [[CrossRef](#)]
23. Zhang, Y.; Zhao, X.; Yang, Q.; Zhang, Z.; Ren, Q.; Xing, H. Long-chain carboxylate ionic liquids combining high solubility and low viscosity for light hydrocarbon separations. *Ind. Eng. Chem. Res.* **2017**, *56*, 7336–7344. [[CrossRef](#)]
24. Mirzaei, M.; Mokhtarani, B.; Badieli, A.; Sharifi, A. Solubility of carbon dioxide and methane in 1-hexyl-3-methylimidazolium nitrate ionic liquid, experimental and thermodynamic modeling. *J. Chem. Thermodyn.* **2018**, *122*, 31–37. [[CrossRef](#)]
25. Shamsuri, A.A. Ionic liquids: Preparations and limitations. *Makara J. Sci.* **2011**, *14*, 102–106. [[CrossRef](#)]
26. Kaur, G.; Kumar, H.; Singla, M. Diverse applications of ionic liquids: A comprehensive review. *J. Mol. Liq.* **2022**, *351*, 118556. [[CrossRef](#)]
27. Welton, T. Ionic liquids: A brief history. *Biophys. Rev.* **2018**, *10*, 691–706. [[CrossRef](#)]
28. Ghandi, K. A review of ionic liquids, their limits and applications. *Green Sustain. Chem.* **2014**, *4*, 44–53. [[CrossRef](#)]
29. Long, Z.; Zhou, X.; Shen, X.; Li, D.; Liang, D. Phase equilibria and dissociation enthalpies of methane hydrate in imidazolium ionic liquid aqueous solutions. *Ind. Eng. Chem. Res.* **2015**, *54*, 11701–11708. [[CrossRef](#)]
30. Maiti, A.; Kumar, A.; Rogers, R.D. Water-clustering in hygroscopic ionic liquids—An implicit solvent analysis. *Phys. Chem. Chem. Phys.* **2012**, *14*, 5139–5146. [[CrossRef](#)]
31. Hawker, R.R.; Haines, R.S.; Harper, J.B. Variation of the cation of ionic liquids: The effects on their physicochemical properties and reaction outcome. *Targets Heterocycl. Syst. Prop* **2015**, *18*, 141–213. [[CrossRef](#)]
32. Anderson, J.L.; Dixon, J.K.; Brennecke, J.F. Solubility of CO<sub>2</sub>, CH<sub>4</sub>, C<sub>2</sub>H<sub>6</sub>, C<sub>2</sub>H<sub>4</sub>, O<sub>2</sub>, and N<sub>2</sub> in 1-Hexyl-3-methylpyridinium Bis (trifluoromethylsulfonyl) imide: Comparison to Other Ionic Liquids. *Acc. Chem. Res.* **2007**, *40*, 1208–1216. [[CrossRef](#)]
33. Treder, N.; Bączek, T.; Wychodnik, K.; Rogowska, J.; Wolska, L.; Plenis, A. The influence of ionic liquids on the effectiveness of analytical methods used in the monitoring of human and veterinary pharmaceuticals in biological and environmental samples—Trends and perspectives. *Molecules* **2020**, *25*, 286. [[CrossRef](#)] [[PubMed](#)]
34. Singh, S.K.; Savoy, A.W. Ionic liquids synthesis and applications: An overview. *J. Mol. Liq.* **2020**, *297*, 112038. [[CrossRef](#)]
35. Karadas, F.; Atilhan, M.; Aparicio, S. Review on the use of ionic liquids (ILs) as alternative fluids for CO<sub>2</sub> capture and natural gas sweetening. *Energy Fuels* **2010**, *24*, 5817–5828. [[CrossRef](#)]
36. Raeissi, S.; Peters, C. High pressure phase behaviour of methane in 1-butyl-3-methylimidazolium bis (trifluoromethylsulfonyl) imide. *Fluid Phase Equilibria* **2010**, *294*, 67–71. [[CrossRef](#)]

37. Jacquemin, J.; Gomes, M.F.C.; Husson, P.; Majer, V. Solubility of carbon dioxide, ethane, methane, oxygen, nitrogen, hydrogen, argon, and carbon monoxide in 1-butyl-3-methylimidazolium tetrafluoroborate between temperatures 283 K and 343 K and at pressures close to atmospheric. *J. Chem. Thermodyn.* **2006**, *38*, 490–502. [[CrossRef](#)]
38. Lei, Z.; Chen, B.; Li, C.; Liu, H. Predictive molecular thermodynamic models for liquid solvents, solid salts, polymers, and ionic liquids. *Chem. Rev.* **2008**, *108*, 1419–1455. [[CrossRef](#)]
39. Finotello, A.; Bara, J.E.; Camper, D.; Noble, R.D. Room-temperature ionic liquids: Temperature dependence of gas solubility selectivity. *Ind. Eng. Chem. Res.* **2008**, *47*, 3453–3459. [[CrossRef](#)]
40. Chen, Y.; Mutelet, F.; Jaubert, J.-N. Solubility of carbon dioxide, nitrous oxide and methane in ionic liquids at pressures close to atmospheric. *Fluid Phase Equilibria* **2014**, *372*, 26–33. [[CrossRef](#)]
41. Bermejo, M.D.; Fieback, T.M.; Martín, Á. Solubility of gases in 1-alkyl-3-methylimidazolium alkyl sulfate ionic liquids: Experimental determination and modeling. *J. Chem. Thermodyn.* **2013**, *58*, 237–244. [[CrossRef](#)]
42. Althuluth, M.; Kroon, M.C.; Peters, C.J. Solubility of methane in the ionic liquid 1-ethyl-3-methylimidazolium tris (pentafluoroethyl) trifluorophosphate. *Ind. Eng. Chem. Res.* **2012**, *51*, 16709–16712. [[CrossRef](#)]
43. Jacquemin, J.; Husson, P.; Majer, V.; Gomes, M.F.C. Low-pressure solubilities and thermodynamics of solvation of eight gases in 1-butyl-3-methylimidazolium hexafluorophosphate. *Fluid Phase Equilibria* **2006**, *240*, 87–95. [[CrossRef](#)]
44. Kumelan, J.; Pérez-Salado Kamps, Á.; Tuma, D.; Maurer, G. Solubility of the single gases methane and xenon in the ionic liquid [bmim][CH<sub>3</sub>SO<sub>4</sub>]. *J. Chem. Eng. Data* **2007**, *52*, 2319–2324. [[CrossRef](#)]
45. Hert, D.G.; Anderson, J.L.; Aki, S.N.; Brennecke, J.F. Enhancement of oxygen and methane solubility in 1-hexyl-3-methylimidazolium bis (trifluoromethylsulfonyl) imide using carbon dioxide. *Chem. Commun.* **2005**, *20*, 2603–2605.
46. Althuluth, M.; Kroon, M.C.; Peters, C.J. High pressure solubility of methane in the ionic liquid 1-hexyl-3-methylimidazolium tricyanomethanide. *J. Supercrit. Fluids* **2017**, *128*, 145–148. [[CrossRef](#)]
47. Liu, X.; Afzal, W.; Yu, G.; He, M.; Prausnitz, J.M. High solubilities of small hydrocarbons in trihexyl tetradecylphosphonium bis (2, 4, 4-trimethylpentyl) phosphinate. *J. Phys. Chem. B* **2013**, *117*, 10534–10539. [[CrossRef](#)] [[PubMed](#)]
48. Yuan, X.; Zhang, S.; Chen, Y.; Lu, X.; Dai, W.; Mori, R. Solubilities of gases in 1, 1, 3, 3-tetramethylguanidium lactate at elevated pressures. *J. Chem. Eng. Data* **2006**, *51*, 645–647. [[CrossRef](#)]
49. Oliveira, L.M.; Ribeiro, F.R.; Alcantara, M.L.; Pisoni, G.O.; Cabral, V.F.; Cardozo-Filho, L.; Mattedi, S. High pressure vapor-liquid equilibria for binary methane and protic ionic liquid based on propionate anions. *Fluid Phase Equilibria* **2016**, *426*, 65–74. [[CrossRef](#)]
50. Alcantara, M.L.; Ferreira, P.I.; Pisoni, G.O.; Silva, A.K.; Cardozo-Filho, L.; Lião, L.M.; Pires, C.A.; Mattedi, S. High pressure vapor-liquid equilibria for binary protic ionic liquids+ methane or carbon dioxide. *Sep. Purif. Technol.* **2018**, *196*, 32–40. [[CrossRef](#)]
51. Cadena, C.; Anthony, J.L.; Shah, J.K.; Morrow, T.I.; Brennecke, J.F.; Maginn, E.J. Why is CO<sub>2</sub> so soluble in imidazolium-based ionic liquids? *J. Am. Chem. Soc.* **2004**, *126*, 5300–5308. [[CrossRef](#)]
52. Bates, E.D.; Mayton, R.D.; Ntai, I.; Davis, J.H. CO<sub>2</sub> capture by a task-specific ionic liquid. *J. Am. Chem. Soc.* **2002**, *124*, 926–927. [[CrossRef](#)]
53. Anthony, J.L.; Maginn, E.J.; Brennecke, J.F. Solubilities and thermodynamic properties of gases in the ionic liquid 1-n-butyl-3-methylimidazolium hexafluorophosphate. *J. Phys. Chem. B* **2002**, *106*, 7315–7320. [[CrossRef](#)]
54. Anthony, J.L.; Anderson, J.L.; Maginn, E.J.; Brennecke, J.F. Anion effects on gas solubility in ionic liquids. *J. Phys. Chem. B* **2005**, *109*, 6366–6374. [[CrossRef](#)] [[PubMed](#)]
55. Baltus, R.E.; Culbertson, B.H.; Dai, S.; Luo, H.; DePaoli, D.W. Low-pressure solubility of carbon dioxide in room-temperature ionic liquids measured with a quartz crystal microbalance. *J. Phys. Chem. B* **2004**, *108*, 721–727. [[CrossRef](#)]
56. Baltus, R.E.; Counce, R.M.; Culbertson, B.H.; Luo, H.; DePaoli, D.W.; Dai, S.; Duckworth, D.C. Examination of the potential of ionic liquids for gas separations. *Sep. Sci. Technol.* **2005**, *40*, 525–541. [[CrossRef](#)]
57. Cammarata, L.; Kazarian, S.; Salter, P.; Welton, T. Molecular states of water in room temperature ionic liquids. *Phys. Chem. Chem. Phys.* **2001**, *3*, 5192–5200. [[CrossRef](#)]
58. Camper, D.; Scovazzo, P.; Koval, C.; Noble, R. Gas solubilities in room-temperature ionic liquids. *Ind. Eng. Chem. Res.* **2004**, *43*, 3049–3054. [[CrossRef](#)]
59. Gomes, M.C.; Padua, A.A. Gas-liquid interactions in solution. *Pure Appl. Chem.* **2005**, *77*, 653–665. [[CrossRef](#)]
60. Husson-Borg, P.; Majer, V.; Costa Gomes, M.F. Solubilities of oxygen and carbon dioxide in butyl methyl imidazolium tetrafluoroborate as a function of temperature and at pressures close to atmospheric pressure. *J. Chem. Eng. Data* **2003**, *48*, 480–485. [[CrossRef](#)]
61. Muldoon, M.J.; Aki, S.N.; Anderson, J.L.; Dixon, J.K.; Brennecke, J.F. Improving carbon dioxide solubility in ionic liquids. *J. Phys. Chem. B* **2007**, *111*, 9001–9009. [[CrossRef](#)] [[PubMed](#)]
62. Scovazzo, P.; Camper, D.; Kieft, J.; Poshusta, J.; Koval, C.; Noble, R. Regular solution theory and CO<sub>2</sub> gas solubility in room-temperature ionic liquids. *Ind. Eng. Chem. Res.* **2004**, *43*, 6855–6860. [[CrossRef](#)]
63. Shiflett, M.B.; Yokozeki, A. Solubilities and diffusivities of carbon dioxide in ionic liquids:[bmim][PF<sub>6</sub>] and [bmim][BF<sub>4</sub>]. *Ind. Eng. Chem. Res.* **2005**, *44*, 4453–4464. [[CrossRef](#)]
64. Shariati, A.; Gutkowski, K.; Peters, C.J. Comparison of the phase behavior of some selected binary systems with ionic liquids. *AIChE J.* **2005**, *51*, 1532–1540. [[CrossRef](#)]
65. Scovazzo, P.; Kieft, J.; Finan, D.A.; Koval, C.; DuBois, D.; Noble, R. Gas separations using non-hexafluorophosphate [PF<sub>6</sub>]<sup>-</sup> anion supported ionic liquid membranes. *J. Membr. Sci.* **2004**, *238*, 57–63. [[CrossRef](#)]

66. Ramdin, M.; Balaji, S.P.; Vicent-Luna, J.M.; Gutiérrez-Sevillano, J.J.; Calero, S.; de Loos, T.W.; Vlugt, T.J. Solubility of the precombustion gases CO<sub>2</sub>, CH<sub>4</sub>, CO, H<sub>2</sub>, N<sub>2</sub>, and H<sub>2</sub>S in the ionic liquid [bmim][Tf<sub>2</sub>N] from Monte Carlo simulations. *J. Phys. Chem. C* **2014**, *118*, 23599–23604. [CrossRef]
67. Zubeir, L.F.; Lacroix, M.H.; Meuldijk, J.; Kroon, M.C.; Kiss, A.A. Novel pressure and temperature swing processes for CO<sub>2</sub> capture using low viscosity ionic liquids. *Sep. Purif. Technol.* **2018**, *204*, 314–327. [CrossRef]
68. Xie, Y.; Zhang, Y.; Lu, X.; Ji, X. Energy consumption analysis for CO<sub>2</sub> separation using imidazolium-based ionic liquids. *Appl. Energy* **2014**, *136*, 325–335. [CrossRef]
69. Zareiekordshouli, F.; Lashanizadehgan, A.; Darvishi, P. Study on the use of an imidazolium-based acetate ionic liquid for CO<sub>2</sub> capture from flue gas in absorber/stripper packed columns: Experimental and modeling. *Int. J. Greenh. Gas Control* **2018**, *70*, 178–192. [CrossRef]
70. Ramdin, M.; de Loos, T.W.; Vlugt, T.J. State-of-the-art of CO<sub>2</sub> capture with ionic liquids. *Ind. Eng. Chem. Res.* **2012**, *51*, 8149–8177. [CrossRef]
71. Kumelan, J.; Pérez-Salado Kamps, Á.; Tuma, D.; Maurer, G. Solubility of the single gases methane and xenon in the ionic liquid [hmim][Tf<sub>2</sub>N]. *Ind. Eng. Chem. Res.* **2007**, *46*, 8236–8240. [CrossRef]
72. Pérez-Salado Kamps, Á.; Tuma, D.; Xia, J.; Maurer, G. Solubility of CO<sub>2</sub> in the ionic liquid [bmim][PF<sub>6</sub>]. *J. Chem. Eng. Data* **2003**, *48*, 746–749. [CrossRef]
73. Jalili, A.H.; Safavi, M.; Ghotbi, C.; Mehdizadeh, A.; Hosseini-Jenab, M.; Taghikhani, V. Solubility of CO<sub>2</sub>, H<sub>2</sub>S, and their mixture in the ionic liquid 1-octyl-3-methylimidazolium bis (trifluoromethyl) sulfonylimide. *J. Phys. Chem. B* **2012**, *116*, 2758–2774. [CrossRef] [PubMed]
74. Jalili, A.H.; Shokouhi, M.; Maurer, G.; Hosseini-Jenab, M. Solubility of CO<sub>2</sub> and H<sub>2</sub>S in the ionic liquid 1-ethyl-3-methylimidazolium tris (pentafluoroethyl) trifluorophosphate. *J. Chem. Thermodyn.* **2013**, *67*, 55–62. [CrossRef]
75. Safavi, M.; Ghotbi, C.; Taghikhani, V.; Jalili, A.H.; Mehdizadeh, A. Study of the solubility of CO<sub>2</sub>, H<sub>2</sub>S and their mixture in the ionic liquid 1-octyl-3-methylimidazolium hexafluorophosphate: Experimental and modelling. *J. Chem. Thermodyn.* **2013**, *65*, 220–232. [CrossRef]
76. Kumelan, J.; Pérez-Salado Kamps, Á.; Tuma, D.; Maurer, G. Solubility of CO<sub>2</sub> in the ionic liquids [bmim][CH<sub>3</sub>SO<sub>4</sub>] and [bmim][PF<sub>6</sub>]. *J. Chem. Eng. Data* **2006**, *51*, 1802–1807. [CrossRef]
77. Wagner, W.; Overhoff, U. *ThermoFluids: Interactive Software for the Calculation of Thermodynamic Properties for More than 60 Pure Substances*; Springer: Berlin/Heidelberg, Germany, 2006.
78. Carvalho, P.J.; Álvarez, V.H.; Machado, J.J.; Pauly, J.; Daridon, J.-L.; Marrucho, I.M.; Aznar, M.; Coutinho, J.A. High pressure phase behavior of carbon dioxide in 1-alkyl-3-methylimidazolium bis (trifluoromethylsulfonyl) imide ionic liquids. *J. Supercrit. Fluids* **2009**, *48*, 99–107. [CrossRef]
79. Valderrama, J.; Robles, P. Critical properties, normal boiling temperatures, and acentric factors of fifty ionic liquids. *Ind. Eng. Chem. Res.* **2007**, *46*, 1338–1344. [CrossRef]
80. Valderrama, J.O.; Rojas, R.E. Critical properties of ionic liquids. Revisited. *Ind. Eng. Chem. Res.* **2009**, *48*, 6890–6900. [CrossRef]
81. Peng, D.-Y.; Robinson, D.B. A new two-constant equation of state. *Ind. Eng. Chem. Fundam.* **1976**, *15*, 59–64. [CrossRef]
82. Song, H.N.; Lee, B.-C.; Lim, J.S. Measurement of CO<sub>2</sub> solubility in ionic liquids: [BMP][TfO] and [P14, 6, 6, 6][Tf<sub>2</sub>N] by measuring bubble-point pressure. *J. Chem. Eng. Data* **2010**, *55*, 891–896. [CrossRef]
83. Chin, H.-Y.; Lee, B.-S.; Chen, Y.-P.; Chen, P.-C.; Lin, S.-T.; Chen, L.-J. Prediction of phase equilibrium of methane hydrates in the presence of ionic liquids. *Ind. Eng. Chem. Res.* **2013**, *52*, 16985–16992. [CrossRef]
84. Smith, J.M. Introduction to chemical engineering thermodynamics. *J. Chem. Educ.* **1950**, *27*, 584. [CrossRef]
85. Sakhaeinia, H.; Taghikhani, V.; Jalili, A.H.; Mehdizadeh, A.; Safekordi, A.A. Solubility of H<sub>2</sub>S in 1-(2-hydroxyethyl)-3-methylimidazolium ionic liquids with different anions. *Fluid Phase Equilibria* **2010**, *298*, 303–309. [CrossRef]
86. Jalili, A.H.; Rahmati-Rostami, M.; Ghotbi, C.; Hosseini-Jenab, M.; Ahmadi, A.N. Solubility of H<sub>2</sub>S in ionic liquids [bmim][PF<sub>6</sub>], [bmim][BF<sub>4</sub>], and [bmim][Tf<sub>2</sub>N]. *J. Chem. Eng. Data* **2009**, *54*, 1844–1849. [CrossRef]
87. Sandler, S.I. *Chemical, Biochemical, and Engineering Thermodynamics*; John Wiley & Sons: Hoboken, NJ, USA, 2017.
88. Elliott, J.R.; Lira, C.T.; Lira, C.T. *Introductory Chemical Engineering Thermodynamics*; Pearson: Prentice Hall Upper, NJ, USA, 2012; Volume 668.
89. Abdul Kareem, F.A.; Shariff, A.M.; Ullah, S.; Garg, S.; Dreisbach, F.; Keong, L.K.; Mellon, N. Experimental and neural network modeling of partial uptake for a carbon dioxide/methane/water ternary mixture on 13X zeolite. *Energy Technol.* **2017**, *5*, 1373–1391. [CrossRef]
90. Eslamimanesh, A.; Gharagheizi, F.; Mohammadi, A.H.; Richon, D. Artificial neural network modeling of solubility of supercritical carbon dioxide in 24 commonly used ionic liquids. *Chem. Eng. Sci.* **2011**, *66*, 3039–3044. [CrossRef]
91. Hamzehie, M.; Fattahi, M.; Najibi, H.; Van der Bruggen, B.; Mazinani, S. Application of artificial neural networks for estimation of solubility of acid gases (H<sub>2</sub>S and CO<sub>2</sub>) in 32 commonly ionic liquid and amine solutions. *J. Nat. Gas Sci. Eng.* **2015**, *24*, 106–114. [CrossRef]
92. Lashkarbolooki, M.; Vaferi, B.; Rahimpour, M. Comparison the capability of artificial neural network (ANN) and EOS for prediction of solid solubilities in supercritical carbon dioxide. *Fluid Phase Equilibria* **2011**, *308*, 35–43. [CrossRef]
93. Oliferenko, A.A.; Oliferenko, P.V.; Seddon, K.R.; Torrecilla, J.S. Prediction of gas solubilities in ionic liquids. *Phys. Chem. Chem. Phys.* **2011**, *13*, 17262–17272. [CrossRef] [PubMed]

94. Safamirzaei, M.; Modarress, H. Hydrogen solubility in heavy n-alkanes; modeling and prediction by artificial neural network. *Fluid Phase Equilibria* **2011**, *310*, 150–155. [[CrossRef](#)]
95. Sedghamiz, M.A.; Rasoolzadeh, A.; Rahimpour, M.R. The ability of artificial neural network in prediction of the acid gases solubility in different ionic liquids. *J. CO<sub>2</sub> Util.* **2015**, *9*, 39–47. [[CrossRef](#)]
96. Safamirzaei, M.; Modarress, H. Correlating and predicting low pressure solubility of gases in [bmim][BF<sub>4</sub>] by neural network molecular modeling. *Thermochim. Acta* **2012**, *545*, 125–130. [[CrossRef](#)]
97. Dashti, A.; Harami, H.R.; Rezakazemi, M.; Shirazian, S. Estimating CH<sub>4</sub> and CO<sub>2</sub> solubilities in ionic liquids using computational intelligence approaches. *J. Mol. Liq.* **2018**, *271*, 661–669. [[CrossRef](#)]
98. Hamed, N.; Rahimpour, M.R.; Keshavarz, P. Methane solubility in ionic liquids: Comparison of cubic-plus-association and modified Sanchez-Lacombe equation of states. *Chem. Phys. Lett.* **2020**, *738*, 136903. [[CrossRef](#)]
99. Loreno, M.; Reis, R.A.; Mattedi, S.; Paredes, M.L. Predicting the solubility of carbon dioxide or methane in imidazolium-based ionic liquids with GC-sPC-SAFT equation of state. *Fluid Phase Equilibria* **2019**, *479*, 85–98. [[CrossRef](#)]
100. Kurnia, K.A.; Matheswaran, P.; How, C.J.; Noh, M.H.; Kusumawati, Y. Solubility of Methane in Alkylpyridinium-Based Ionic Liquids at Temperatures between 298.15 and 343.15 K and Pressures up to 4 MPa. *J. Chem. Eng. Data* **2020**, *65*, 4642–4648. [[CrossRef](#)]
101. Kurnia, K.A.; How, C.J.; Matheswaran, P.; Noh, M.H.; Alamsjah, M.A. Insight into the molecular mechanism that controls the solubility of CH<sub>4</sub> in ionic liquids. *New J. Chem.* **2020**, *44*, 354–360. [[CrossRef](#)]
102. Elhenawy, S.; Khraisheh, M.; AlMomeni, F.; Hassan, M. Key applications and potential limitations of ionic liquid membranes in the gas separation process of CO<sub>2</sub>, CH<sub>4</sub>, N<sub>2</sub>, H<sub>2</sub> or mixtures of these gases from various gas streams. *Molecules* **2020**, *25*, 4274. [[CrossRef](#)] [[PubMed](#)]
103. do Nascimento, D.C.; Pelaquim, F.P.; Bertocin, T.A.; Neto, A.M.B.; da Costa, M.C. Thermodynamic modeling of methane hydrate equilibrium conditions in the presence of imidazolium based ionic liquids with the Waals-Platteeuw solid solution approach along with SRK and CPA EoS. *Fluid Phase Equilibria* **2023**, *571*, 113822. [[CrossRef](#)]

**Disclaimer/Publisher's Note:** The statements, opinions and data contained in all publications are solely those of the individual author(s) and contributor(s) and not of MDPI and/or the editor(s). MDPI and/or the editor(s) disclaim responsibility for any injury to people or property resulting from any ideas, methods, instructions or products referred to in the content.